ISTITUTO NAZIONALE DI FISICA NUCLEARE

Sezione di Milano

INFN/AE–94/01
7 Gennaio 1994

F.W. Bopp, E. Engel, D. Pertermann, J. Ranft:

NEW PARTON STRUCTURE FUNCTIONS AND MINIJETS IN THE TWO–COMPONENT DUAL PARTON MODEL

PACS: 13.85.Hd ; 12.40.Aa ; 12.40.Lk

Servizio Documentazione
dei Laboratori Nazionali di Frascati

INFN – Istituto Nazionale di Fisica Nucleare
Sezione di Milano

INFN/AE–94/01
7 Gennaio 1994

NEW PARTON STRUCTURE FUNCTIONS AND MINIJETS IN THE TWO–COMPONENT DUAL PARTON MODEL

F.W.Bopp, [a] R.Engel, [b] D.Pertermann [c] and J.Ranft[d]

[a]Fachbereich Physik, Universität Siegen, D–57068 Siegen, F.R.G.

[b]Fachbereich Physik, Universität Leipzig, D–04109, Leipzig, F.R.G.

[c]Fachbereich Physik, Universität Siegen, D–57068 Siegen, F.R.G.

[d]INFN, Sezione di Milano, Via Celoria 16, I–20133 Milano, Italy

We use new fits to parton structure functions, including structure functions with Lipatov behaviour at small x–values and discuss the minijet component in the two–component Dual Parton Model with a supercritical Pomeron as demanded by the fits to cross section data. We find, that a consistent model can only be formulated with a $p_{\perp thr}$ cut–off for the minijets increasing with energy. The implications for particle production in hadronic collisions at TeV energies are discussed.

1. Introduction

Soft multiparticle production characterizing hadronic interactions energies cannot be understood purely within theoretical approaches provided by perturbative QCD. The nonperturbative soft component of hadron production, which is responsable for all of hadron production at low energies is still acting at present and future collider energies.

Using basic ideas of the dual topological unitarization scheme[1,2] the Dual Parton Model (DPM) (a recent review is given in Ref.[3]) has been very successfully describing soft hadronic processes. Several new features of $p\bar{p}$ collisions at collider energies which were subsequently confirmed by experiments, could be anticipated.

Observations like rapidity plateaus and average transverse momenta rising with energy, KNO scaling violation, transverse momentum–multiplicity correlations and *minijets* pointed out, that soft and hard processes are closely related. These properties were understood within the two–component Dual Parton Model.[4-9]

The hard component is introduced applying lowest order of perturbative hard constituent scattering.[10] Single diffraction dissociation is represented by a triple–Pomeron exchange (high mass single diffraction) and a low mass component.

The Monte–Carlo implementation of the Dual Parton Model (DTUJET[5] for hadron–hadron collisions) enables us to investigate the predictions given by the model at energies of present and future hadron colliders. In the present paper we discuss mainly the minijet component. This is appropriate, since the first results from HERA on deep inelastic scattering at low x[11] seem to indicate, that the structure functions at low x rise much stronger than anticipated in the past by most of the conventional structure function parametrizations. We will see, that this, if also found for the gluon structure function, can lead to dramatic consequences for the minijet component.
In Section 2 we give a short account of the two–component Dual Parton Model, in Section 3 we give details about the parton structure functions used to calculate the minijet cross sections, in Section 4 and 5 study the model with an energy independent cut–off for the minijets, we fit the parameters of the model to cross–section data and study the phenomenology of the resulting model. In Sections 6 and 7 we study the model with an energy dependent cut–off for the minijets and we investigate the multiparticle production in the resulting model In Section 8 we give a Summary.

2. The two–component Dual Parton Model

The soft input cross section in our unitarization scheme is described by the supercritical Pomeron

$$\sigma_s = g^2 s^{\alpha(0)-1} \tag{1}$$

with g being the effective proton–Pomeron coupling constant and $\alpha(0)$ the Pomeron intercept. The corresponding Pomeron–trajectory is given by $\alpha(t) = \alpha(0) + \alpha' t$. The supercritical Pomeron was used in the two–component DPM from the beginning,[4] while other approaches use the critical Pomeron with $\alpha(0) = 1$ from Durand and Pi[12] up to HIJING.[13] A large part of the differences between HIJING and the DPM–results is due to this different starting point. In all fits of the Pomeron parameters to cross section data including the ones, we will report here, we get consistently better fits with the supercritical Pomeron than with the critical one.

These better fits to the supercritical Pomeron are one of our arguments for the continuous presence of the soft component to multiparticle production in the TeV energy region.

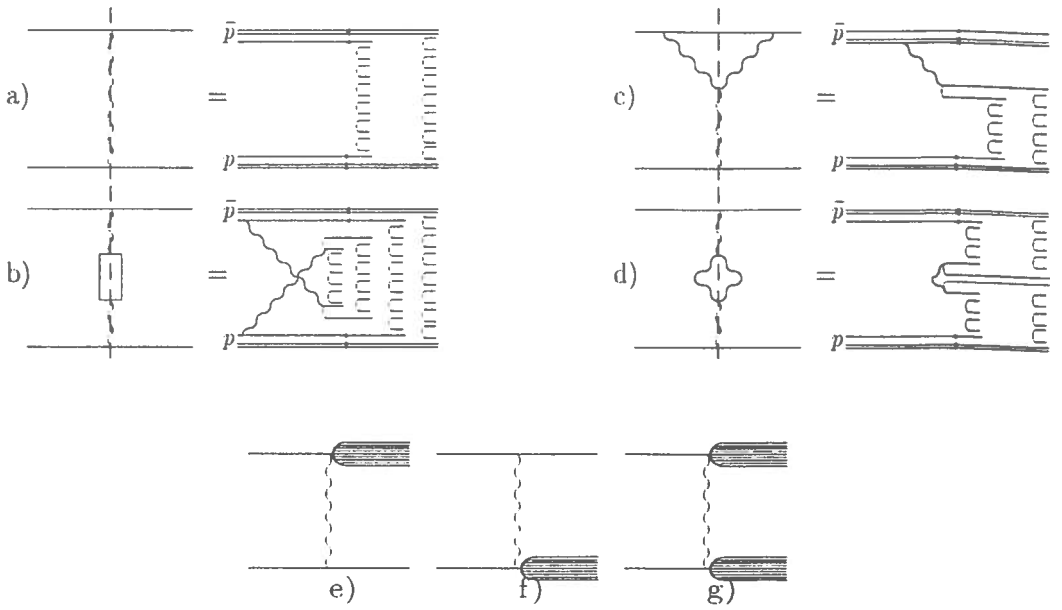

Figure 1. Diagrams and the corresponding cut graphs for the exchange of a) one soft Pomeron, b) one hard Pomeron, and c) one triple–Pomeron (high mass single diffraction). Fig. d) shows one cut Pomeron–loop graph (high mass double diffraction). Low mass single diffractive processes (e),(f) and low mass double diffractive processes (g) are introduced via a two–channel eikonal formalism

Furthermore we introduce graphs with Pomeron–Pomeron couplings. Provided that the Pomeron–Pomeron coupling constant Γ is small in comparison with other couplings, such as g, it is sufficient to consider the expansion in Γ only up to first order[5] . Thus a correction to the pure Pomeron–exchange is represented by the triple–Pomeron graph (Fig. 1(c)). included with an input cross section

$$\sigma_{TP} = \frac{2}{16\pi}\frac{g^3\Gamma}{b_{sd}} ln\frac{s}{s_0} \tag{2}$$

where b_{sd} is the slope $b_{sd} = b^0_{sd} + 2\alpha' ln(s)$, $b^0_{sd} = 3.7\ GeV^{-2}$, $\alpha' = 0.24\ GeV^{-2}$ and $s_0 = 100\ GeV^2$. (The numbers given here are the ones used in the published model,[5] in Section 4 we will determine these parameters for the model presented here in fits to cross–section data.) The simplest cut of the triple–Pomeron (Fig. 1(c)) corresponds to a high mass single diffractive interaction. High mass diffraction is a comparable rare process. High mass means that the diffractively excited system should not be a well defined hadron resonance. We also describe high mass double diffractive processes again to first order introducing loop graphs (Fig. 1(d)), with a cross section

$$\sigma_L = \frac{1}{16\pi}\frac{g^2\Gamma^2}{2b_{DD}}(ln^2\frac{s}{s_0} + ln^2\frac{s'_0}{s} - 2ln^2\frac{5}{20}) \tag{3}$$

with b_{DD} being the slope parameter $b_{DD} = 2\alpha' ln(s)$, $s_0 = 400\ GeV^2$, and $s'_0 = 25\ GeV^2$.

The input cross section for semihard multiparticle production σ_h is calculated applying the QCD improved parton model as described in Ref..[14, 4, 7, 8]

$$\sigma_h = \sum_{i,j} \int_0^1 dx_1 \int_0^1 dx_2 \int d\hat{t}\ \frac{1}{1+\delta_{ij}} \frac{d\sigma_{QCD,ij}}{d\hat{t}}\ f_i(x_1,Q^2) f_j(x_2,Q^2)\ \Theta(p_\perp - p_{\perp thr}) \quad (4)$$

$f_i(x,Q^2)$ are the structure functions of partons with the flavor i and scale Q^2 and the sum i,j runs over all possible flavors. To remain in the region where perturbation theory is valid, we use a low $p_\perp$ cut–off $p_{\perp_{thr}}$ for the minijet component. Furthermore, since we calculate $\sigma_{QCD,ij}$ in lowest-order QCD perturbation theory we multiply the hard input cross section σ_h with a K factor in the range of 1.5 to 2. A hard interaction leads to a chain system shown in Fig. 1(b).

The momentum fractions of the constituents at the ends of the different chains are sampled using the exclusive parton distribution, which has the form for an event with n_s soft and $n_h (n_h \geq 1)$ hard Pomerons

$$\rho(x_1,...,x_{2n_s},...,x_{2n_s+2+n_h}) \sim \frac{1}{\sqrt{x_1}} \Big(\prod_{i=3}^{2n_s+2} \frac{1}{x_i}\Big) x_2^{1.5} \prod_{i=2n_s+3}^{2n_s+2+n_h} g(x_i,Q_i)\,\delta\Big(1 - \sum_{i=1}^{2n_s+2+n_h} x_i\Big). \quad (5)$$

The distributions $g(x_i,Q_i)$ are the distribution functions of the partons engaged in the hard scattering.

Soft(s), hard(h), high mass single diffractive(TP), and high mass double diffractive(L) processes are treated simultaneously within an eikonal unitarization scheme using the impact parameter representation

$$\chi_i(B,s) = \frac{\sigma_i(s)}{8\pi b_i} \exp[-\frac{B^2}{4b_i}], \qquad i = s,h,TP,L \quad (6)$$

normalized by

$$\int 2\chi_i(B,s)\, d^2B = \sigma_i \quad (7)$$

with $b_h = b, b_s = b_{TP} = b_L = b + \alpha' log(s)$. The exclusive cross section for l_c cut soft Pomerons, m_c cut hard Pomerons, n_c cut triple–Pomeron graphs and p_c cut loop graphs is given by

$$\sigma(l_c,m_c,n_c,p_c,B,s) = \frac{(2\chi_s)^{l_c}}{l_c!} \frac{(2\chi_h)^{m_c}}{m_c!} \frac{(-2\chi_{TP})^{n_c}}{n_c!} \frac{(-2\chi_L)^{p_c}}{p_c!} \exp[-2\chi(B,s)] \quad (8)$$

with

$$\chi(B,s) = \chi_s(B,s) + \chi_h(B,s) - \chi_{TP}(B,s) - \chi_L(B,s). \quad (9)$$

The total and elastic cross section are given by

$$\sigma_{tot} = 4\pi \int_0^\infty BdB(1 - \exp[\chi(B,s)]), \quad \sigma_{el}(B,s) = \frac{1}{4}[\sigma_{tot}(B,s)]^2. \quad (10)$$

Diffractive processes characterized by the excitation of an initial hadron to intermediate resonances (low mass diffractive interactions) are introduced via a two channel eikonal formalism. As suggested in Ref.[5] a new coupling λ modifies the three graphs given in Fig. 1(e-g) and leads to a modification of each graph with l soft, m hard, n triple–Pomeron, and p loop exchanges.

The low mass (LMSD) and high mass (HMSD) single diffractive cross sections are given[6] by (the definitions for the $\sigma^{(i)}$ and $\chi(i)$ are given in Ref.[5]).

$$\sigma_{LMSD}(B,s) = \frac{1}{8}(\exp[-\chi^{(1)}(B,s)] - \exp[-\chi^{(2)}(B,s)])^2, \tag{11}$$

$$\begin{aligned}\tilde{\sigma}_{HMSD}(B,s) &= \frac{1}{4}\sum_{i=1}^{4}\tilde{\sigma}^{(i)}_{HMSD} \\ &= \frac{1}{4}\sum_{i=1}^{4}(\exp[\chi^{(i)}_{TP}(B,s)] - 1)\exp[-2\chi^{(i)}(B,s)]\end{aligned} \tag{12}$$

with $\tilde{\sigma}_{HMSD} = \sigma_{HMSD} + \sigma_{HMLMSD}$ (high mass–low mass single diffraction).

3. Current parametrizations of parton structure functions

During 1992–3 new data on deep inelastic scattering and new fits to parton structure functions were reported. New features of these fits include (i) the flavor dependence of sea–quark distributions and (ii) a stronger rise of the structure functions at low x–values, that is in the region important for minijets. These fits by Martin Roberts and Stirling[15] and by the CTEQ–Collaboration[16] include functions with a conventional $1/x$ singularity of sea–quark and gluon distributions (for instance the MRS[D–0] functions) as well as functions with a $1/x^{1.5}$ singularity (for instance the MRS[D–] functions). The pre–HERA measurements do not allow to decide between these two possibilities. However, there are theoretical arguments in favor of the $1/x^{1.5}$ singularity.[17] These more singular parton distributions were in the past used to calculate the minijets,[7,8] but not taken very seriously. This has now to be changed, since the first HERA–data seem to favor just these singular parton distribution functions.[11]

Gluons are the most important source of minijets, unfortunately, so far no HERA data for the gluon distributions are available, but we should start now to discuss the implementation of the more singular functions for minijets.

4. Determining the free parameters of the model in fits to cross–section data, DTUJET92, energy independent cut–off $p_{\perp,thr}$

We describe these fits and the resulting model (similar fits were already reported in[7,8]) without much detail. As in the past, we use two different cut–off's for the minijets $p_{\perp thr} = 2$ and 3 GeV/c. In Tables 1 and 2 we give the results of the fit, that are the optimal model parameters determined.

Table 1
Model parameters obtained with a $p_{\perp}^{cut-off}$ of 3 GeV/c. In the last column the χ^2 values divided by the degrees of freedom (DF) are listed.

PDF set	$g^2(mb)$	$\alpha(0)$	λ	χ^2/DF
MRS[D0]	52.9 ± 1.3	1.073 ± 0.003	0.73 ± 0.02	5.5
MRS[D-]	54.4 ± 1.4	1.069 ± 0.003	0.72 ± 0.02	4.8
CTEQ 1M	52.4 ± 1.3	1.074 ± 0.002	0.74 ± 0.02	5.0
CTEQ 1MS	52.4 ± 1.4	1.074 ± 0.002	0.74 ± 0.02	4.9
CTEQ 1ML	53.3 ± 1.3	1.072 ± 0.003	0.73 ± 0.02	4.6
CTEQ 1L	51.8 ± 1.4	1.076 ± 0.002	0.74 ± 0.02	5.1

Table 2
Model parameters obtained with a $p_{\perp}^{cut-off}$ of 2 GeV/c. In the last column the χ^2 values divided by the degrees of freedom (DF) are listed.

PDF set	$g^2(mb)$	$\alpha(0)$	λ	χ^2/DF
MRS[D0]	68.5 ± 1.0	1.029 ± 0.002	0.58 ± 0.01	1.1
MRS[D-]	63.1 ± 1.1	1.049 ± 0.002	0.68 ± 0.02	3.2
CTEQ 1M	60.8 ± 1.2	1.051 ± 0.003	0.67 ± 0.03	2.1
CTEQ 1MS	61.3 ± 1.1	1.053 ± 0.003	0.67 ± 0.02	2.1
CTEQ 1ML	64.5 ± 1.3	1.042 ± 0.002	0.64 ± 0.02	1.4
CTEQ 1L	57.2 ± 1.4	1.060 ± 0.003	0.70 ± 0.02	3.1

In the fits we use the new structure function sets MRS[D–0] and MRS[D–][15] and the corresponding CTEQ functions.[16] Using the MRS structure functions we use the scale $Q^2 = p_\perp^2/4$ like in our previous papers, but in the case of the CTEQ structure functions we chose a different scale $Q^2 = p_\perp^2$. This different choice is required in order to remain in the Q^2 range of the parametrizations. For all considered parton distributions we obtained acceptable fits and acceptable descriptions of the data.

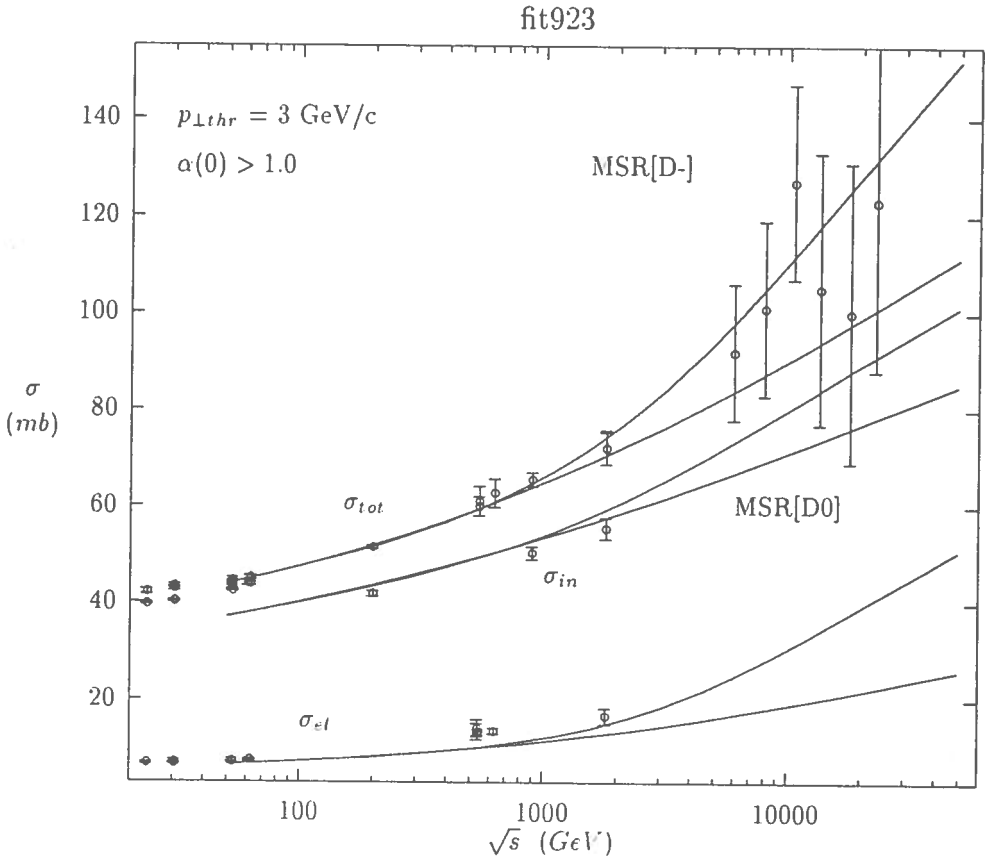

Figure 2. Cross sections σ_{tot}, σ_{el}, and σ_{in} , compared with the two-component DPM DTUJET92 .

In Figs. 2 and 3 for the MRS stucture functions we compare the calculated cross sections to the data from ISR to Tevatron energies. The data for total and elastic cross sections used in the fits and plotted in Figs. 2 and later Figs. are from Refs..[18–23] The data for diffractive cross sections used in the fits and plotted in Figs. 3 and later Figs. are from Refs..[24–28, 23, 29] Not used in the fits but included in the plots are cosmic ray data.[30, 31] The fit results (see Tables 1 and 2) show that $\alpha(0)$ always corresponds to a supercritical soft Pomeron. Using the CTEQ structure functions we get an greement with the cross sections comparable to the fits to the MRS structure

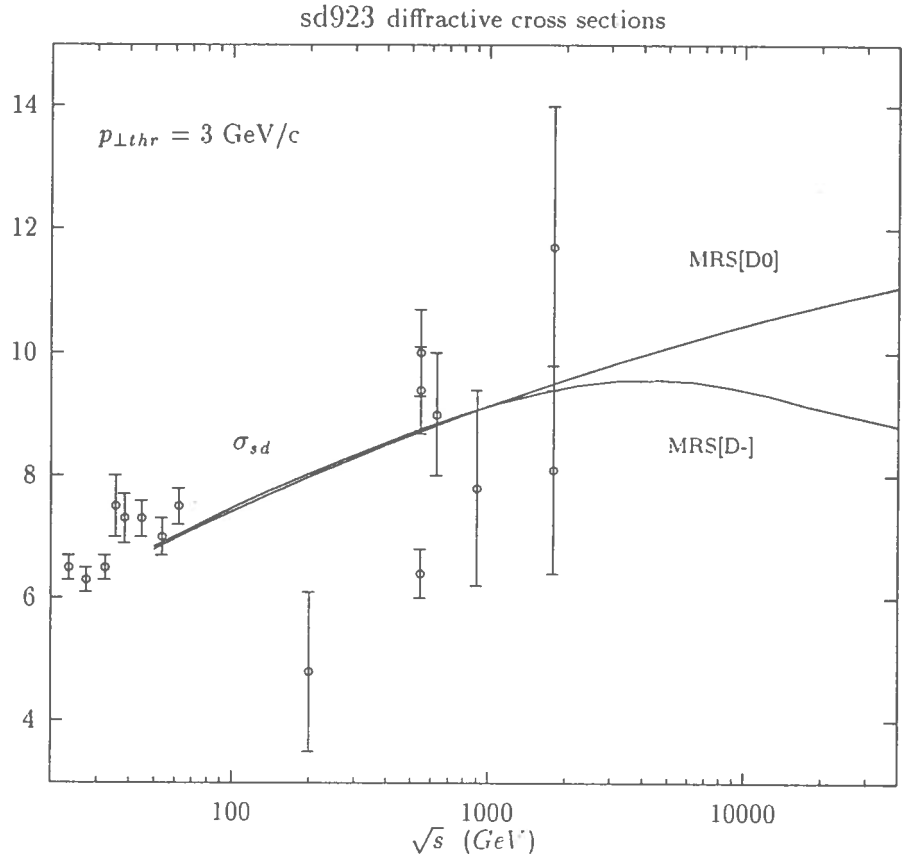

Figure 3. Cross section σ_{diff} . compared with the two-component DPM DTU-JET92 .

functions, Due to the uncertainties of the parton distributions at low x-values the extrapolation already of all these cross -sections to high energies is rather difficult. We are not able to give an unique prediction of the behaviour of the cross sections at supercollider energies. The reason for this are the input minijet cross sections, which we calculate using the two different parton distributions: We obtain at $\sqrt{(s)} = 40$ TeV approximately with MRS[D–0] $\sigma_h = 200$ mb and with MRS[D-] σ_h =1200 mb. The unitarization method compensates for most of the difference and gives output values of σ_{tot} of about 120 and 160 mb. respectively. If we calculate the rapidity distributions in the two models the differences are much bigger.

5. DTUJET92 phenomenology

In Fig.4 we plot rapidity distributions obtained using the MRS[D–0] structure functions and compare to experimental data.

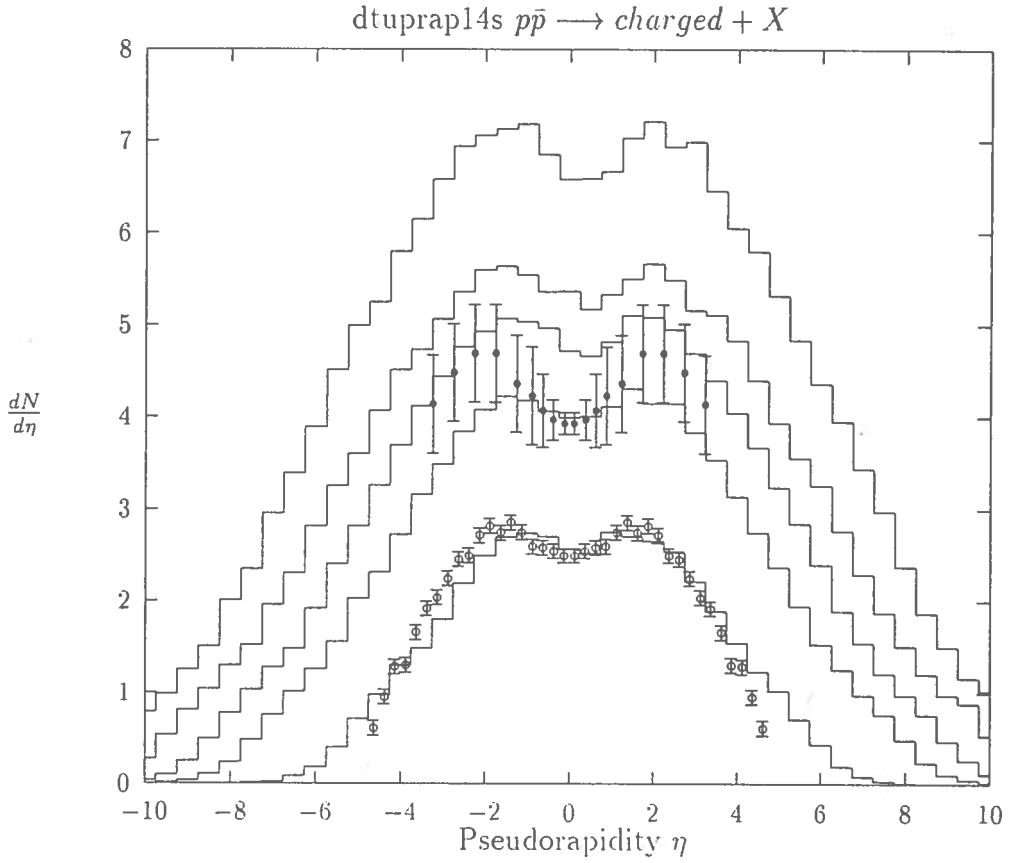

Figure 4. Pseudorapidity distributions in DTUJET92 with MRS[D–0], compared to collider data[37,38] and extrapolated to TeV energies . From top to bottom the energies are: $\sqrt{s}$ = 40 TeV, 14.6 TeV, 5 TeV, 1.8 TeV, 0.2 TeV.

In Fig.5 we plot the central pseudorapidity plateau as function of the energy for three models, up to present collider energies both models agree with each other and with the experimental data but in the super collider energy region the differences are very big.

At present CERN and TEVATRON collider energies, there is nothing wrong with this model and indeed, DTUJET92, with JETSET[32] fragmentation and parton evolution gives with all MRS-92 and CTEQ PDF's an excellent phenomenology. See Fig.4, where we compare with pseudorapidity distributions,Fig.6, where we compare with transverse momentum distributions, Fig.7, where we compare with transverse

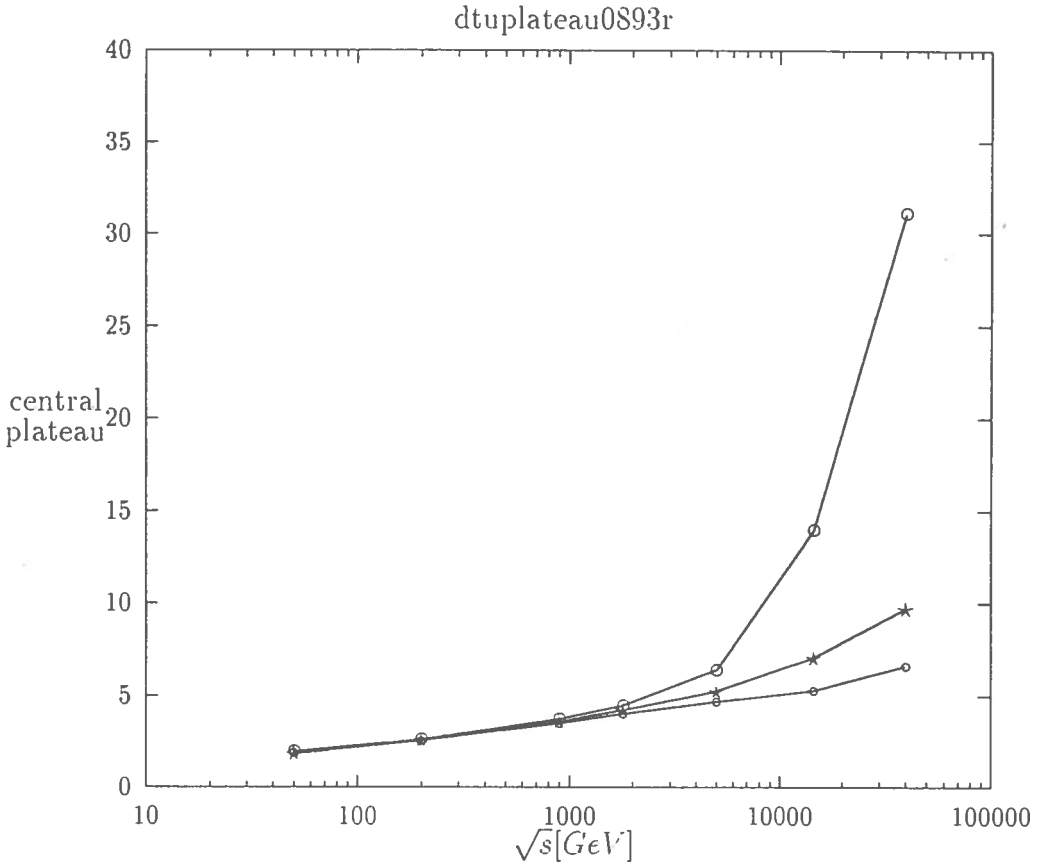

Figure 5. Rise of the pseudorapidity plateau in DTUJET92. The curves from top to bottom are for the structure functions MRS[D–], CTEQ[1ML] and MRS[D–0].

energy distributions or Fig.8, where we compare with average transverse momentum—multiplicity correlatins for produced pions and antiprotons.

At these energies the model is still consistent, since the minijet cross sections are small.

In Fig.5 we plot the rise of the pseudorapidity plateau in this model with different structure functions. We see, extrapolating with MRS[D–] into the ten of TeV energy region, the model becomes inconsistent and produces unreliable results like a pseudorapidity plateau at the energy of 40 TeV of 30-35 charged hadrons per pseudorapidity unit, while previous versions of the model and the same model with conventional PDF's give plateaus between 6 and 8 charged particles per pseudorapidity unit.

At these energies and with the MRS[D–] structure function the DTUJET92 model has become inconsistent and is wrong.

What is inconsistent and wrong: The input minijet cross sections σ_h, which we put so far into the unitarization scheme are inclusive cross sections normalized to

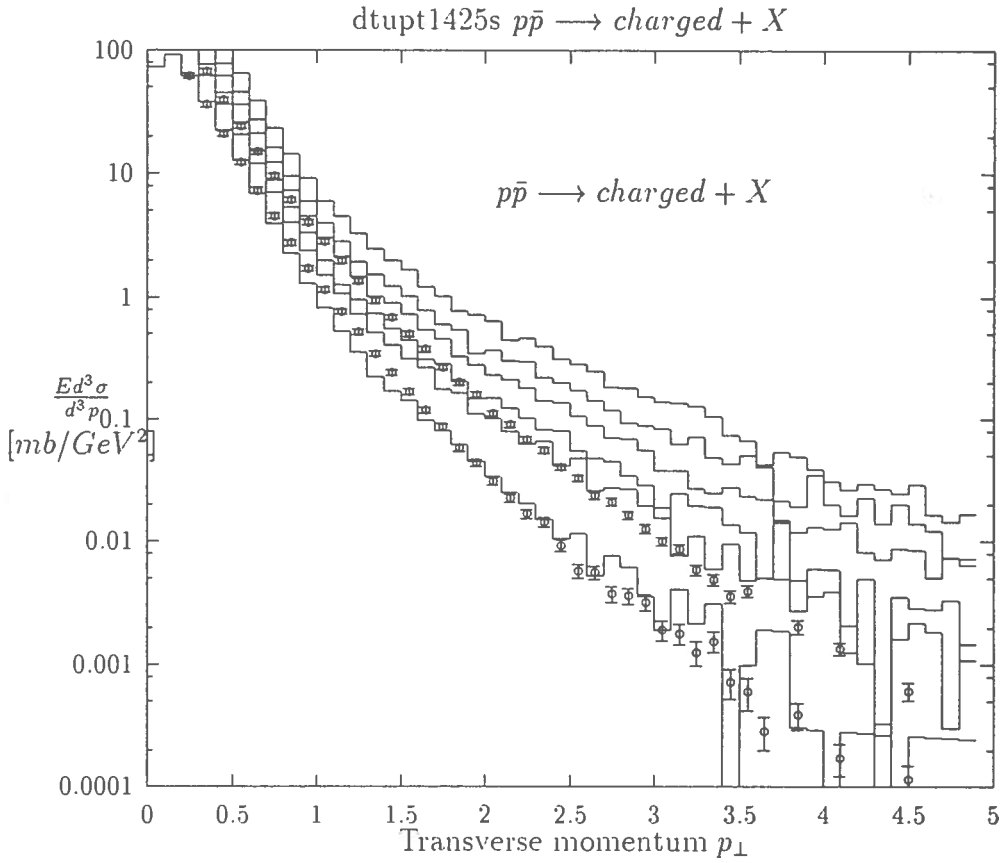

Figure 6. Comparison of transverse momentum distributions with collider data.[39] The energies are from top to bottom: $\sqrt{s}$ = 40 TeV, 14.6 TeV, 5 TeV, 1.8 TeV, 0.9 TeV and 0.2 TeV.

$n_{minijets}\sigma_{inel}$, where $n_{minijets}$ is the multiplicity of minijets. But the physical processes, which contribute to this inclusive cross section, if we use parton distributions with Lipatov behaviour, are $2 \to n$ parton processes, in Fig.9 we give such a typical process. $2 \to n$ processes give a contribution to σ_h equal to $n\sigma_{2\to n}$. Furthermore, the s–channel iteration of such a huge cross section is probably incorrect. If we treat this huge cross section as σ_h in the usual way in the eikonal unitarization scheme we replace it by $n/2$ simultaneuos $2 \to 2$ parton processes like the one given in Fig.10, this is the inconsistency. What we should really use in the unitarization, but what we do not know how to compute reliably at present would be

$$\sigma_h = \sum_n \sigma_{2\to n} \tag{13}$$

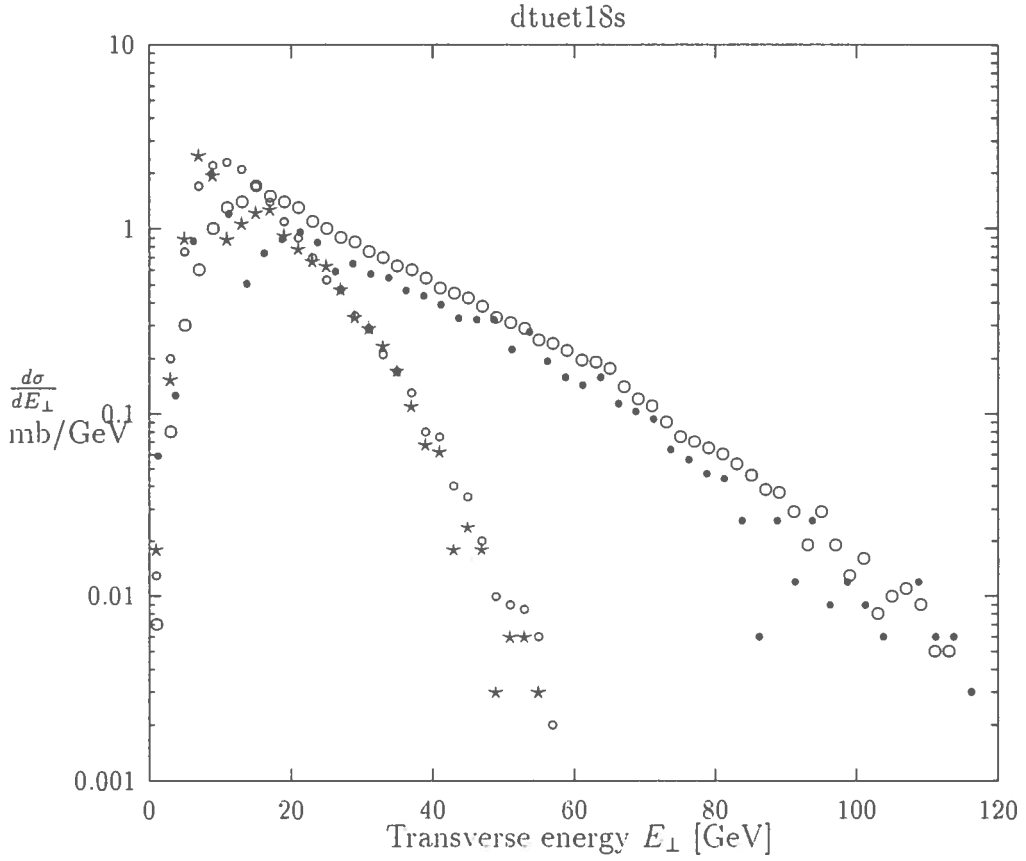

Figure 7. Comparison of transverse Energy distributions with collider data[39]. Open symbols: experimental data, solid symbols: DTUJET92. Upper curves: $\sqrt{s} = 900$ GeV, lower curves: $\sqrt{s} = 200$ GeV.

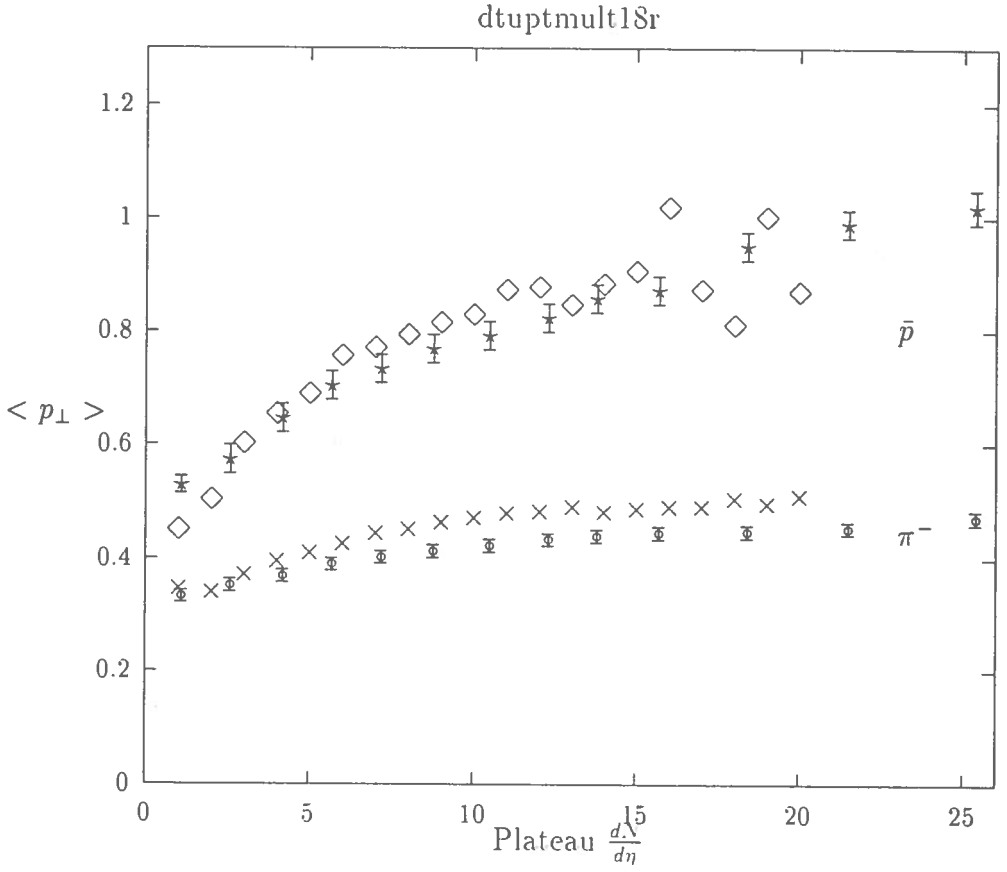

Figure 8. Comparison of average transverse momentum – multiplicity correlations with collider data.[41] The calculated values are without, the experimental data are with errorbars.

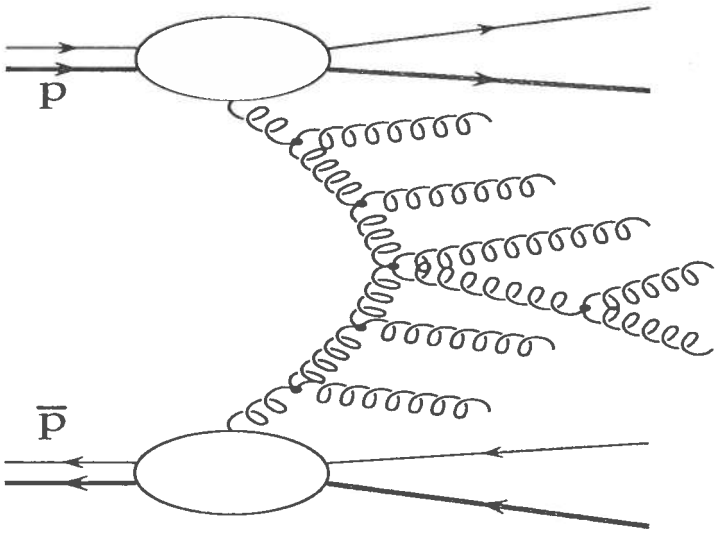

Figure 9. A typical process, where n minijets are produced.

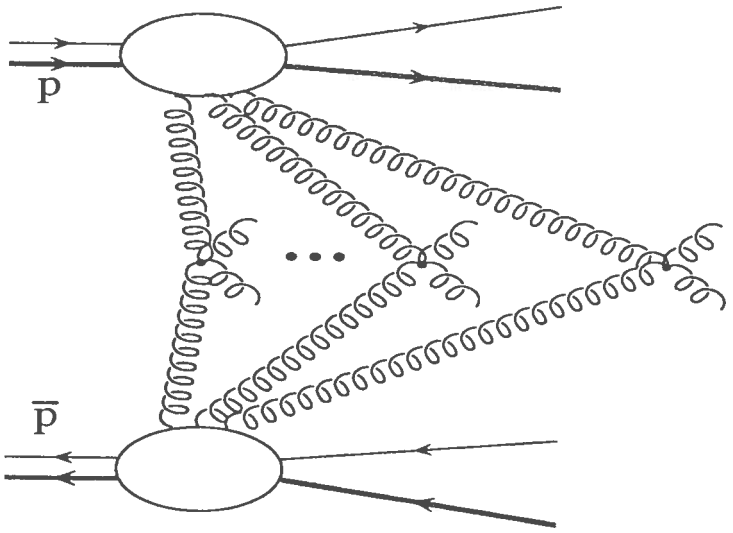

Figure 10. The eikonalization gives n simultaneous $2 \to 2$ parton processes.

6. Determining the free parameters of the model in fits to cross–section data, DTUJET93, energy dependent cut–off $p_{\perp,thr}$

The way to remove this inconsistency is to make in DTUJET-93 the threshold for minijet production $p_{\perp thr}$ energy dependent in such a way, that at no energy and for no PDF the resulting σ_h is bigger than the total cross section. Then at least we have a cross section, which is indeed mainly the cross section of a $2 \rightarrow 2$ parton process at this level, but we can get back to the real $2 \rightarrow n$ processes via parton showering. One possible form for this energy dependent cut off is:

$$p_{\perp thr} = 2.5 + 0.12[\lg_{10}(\sqrt{s}/\sqrt{s_0})]^3 \quad [GeV/c], \quad \sqrt{s_0} = 50GeV. \tag{14}$$

The resulting σ_h are smaller than the total cross sections resulting after the unitarization for all MRS-92 and CTEQ PDF's and also the older KMRS[33] distributions. We note, that this energy dependent $p_\perp$ cut–off corresponds numerically closely to the one used by Geiger,[34-36] but the physical motivation for its use is of course completely different.

Now we are again consistent.

Table 3
DTUJET93 model parameters obtained with an energy dependent $p_{\perp thr}$.

PDF set	$g^2(mb)$	$\alpha(0)$	$\alpha' [GeV^{-2}]$	$b [GeV^{-2}]$	$b_h [GeV^{-2}]$	λ
MRS[D–0]	49.14	1.0636	0.173	1.63	4.01	0.565
MRS[D–]	55.96	1.0490	0.351	1.038	2.01	0.584
CTEQ[1M]	50.85	1.0589	0.210	1.516	3.44	0.562
CTEQ[1MS]	52.25	1.0560	0.256	1.365	2.96	0.574
CTEQ[1ML]	53.73	1.0489	0.250	1.390	2.83	0.529
CTEQ[1DIS]	49.85	1.0616	0.188	1.583	3.75	0.565
CTEQ[1L]	49.56	1.0614	0.208	1.520	3.81	0.593

We use as first described in[14] at $p_{\perp thr}$ the continuity requirement for the *soft* and *hard* chain end $p_\perp$ distributions. Physically, this means, that we use the soft cross section to cut the singularity in the minijet $p_\perp$ distribution. But note, that this cut moves with rising collision energy to higher and higher $p_\perp$ values. This procedure has besides cutting the singularity more attractive features:

(i) The model results (at least as long as we do not violate the consistency requirement described above) become largely independent from the otherwise arbitrary $p_\perp$ cut–off. This was already demonstrated with DTUJET90[5] and cut–offs of 2 and 3 GeV/c. This property is also seen in the present paper, we need only compare results obtained with conventional structure functions with DTUJET92 and DTUJET93, which differ drastically in the prescription for the $p_\perp$ cut–off.

(ii)The continuity between soft and semihard physics is emphasized, there is no basic difference between soft and semihard chains besides the technical problem, that perturbative QCD allows only to calculate the semihard component.

(iii) With this continuity in mind we feel free to call all chain ends, whatever their origin in the model, minijets, as soon as their $p_\perp$ exceeds a certain value, say 2 GeV/c.

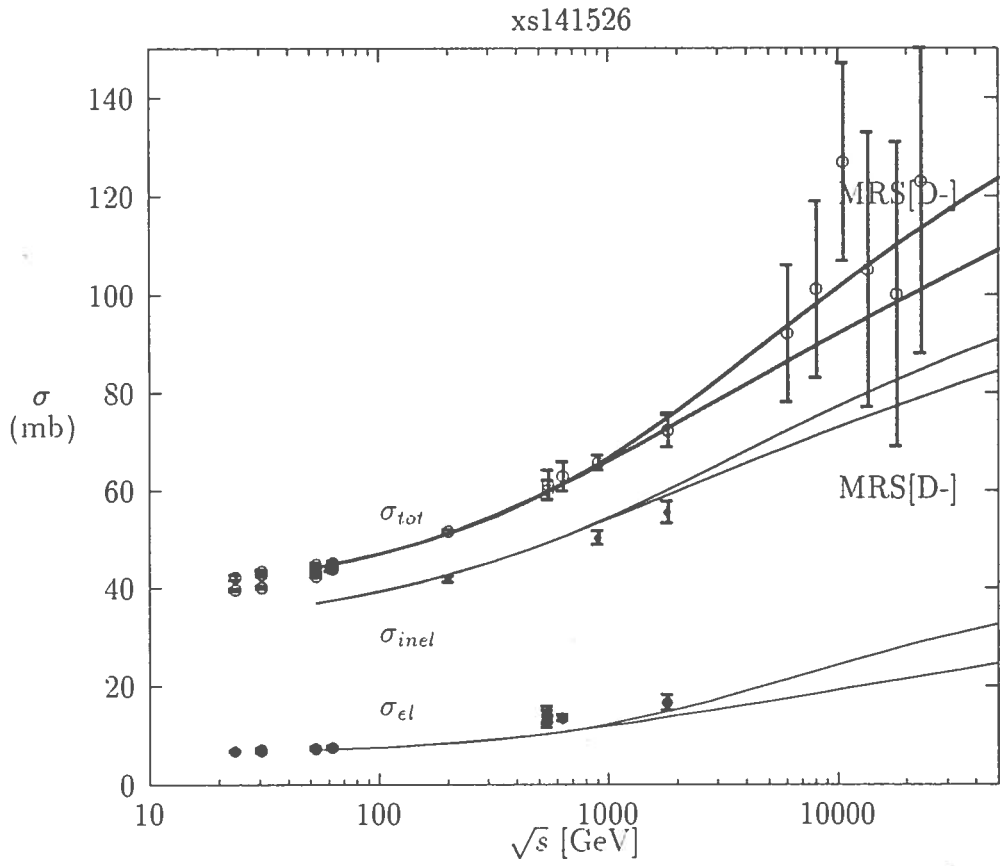

Figure 11. Cross sections σ_{tot}, σ_{el}, and σ_{in}, compared with the two-component DPM DTUJET93. (MRS[D–0] and MRS[D–])

We turn now to the fit of the Pomeron parameters in the case of DTUJET93 with the energy dependent $p_\perp$ cut–off given above. To describe the high energy particle production we have to determine the free parameters of the model, i.e. the proton-Pomeron coupling constant g, the effective soft Pomeron intercept $\alpha(0)$, the slope of the Pomeron trajectory α', the slope parameters b and b_h and the excitation coupling constant λ. This has been done by a global fit to all available data of total, elastic, inelastic, and single diffractive cross sections in the energy range from ISR to collider experiments as well as to the data on the elastic slopes in this energy range. Since

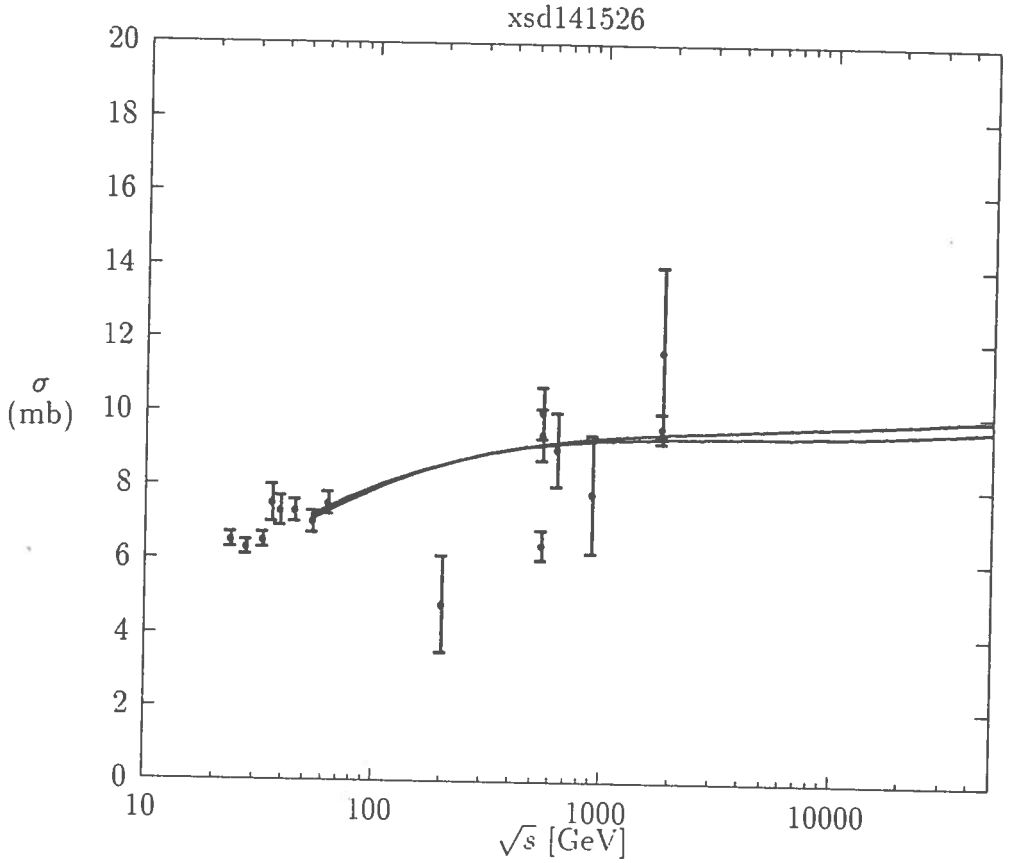

Figure 12. Cross sections σ_{diff} compared with the two-component DPM DTU-JET93. (MRS[D–0] and MRS[D–])

there are large differences in the hard parton distribution functions at small x values resulting in different hard input cross sections we have to perform separate fits for each set of parton distribution functions.

We get again good fits using all of the PDF's, which also as before give us a supercritical Pomeron, not a critical one. In Table 3 we give the parameters obtained in the fit. All the values obtained for $\alpha(0)$ demonstrate again that the fits result in a supercritical Pomerom. In Figs. 11 and 12 we plot the fitted cross sections obtained with the MRS–92 PDF's together with the data, in Figs.13 the same is done for three of the CTEQ parton distributions. The single diffractive cross sections obtained using the CTEQ parton distributions agree practically with the ones in Fig.12. We note, that the differences of the output σ_{tot} obtained with the conventional MRS[D–0] and the Lipatov behaved MRS[D–] structure functions are much smaller than in the fit with constant $p_{\perp thr}$.

In order to demonstrate the continuity of soft and semihard chain end $p_\perp$ distributions we plot in Figs.14 and 15 always at three energies the numbers of chain ends

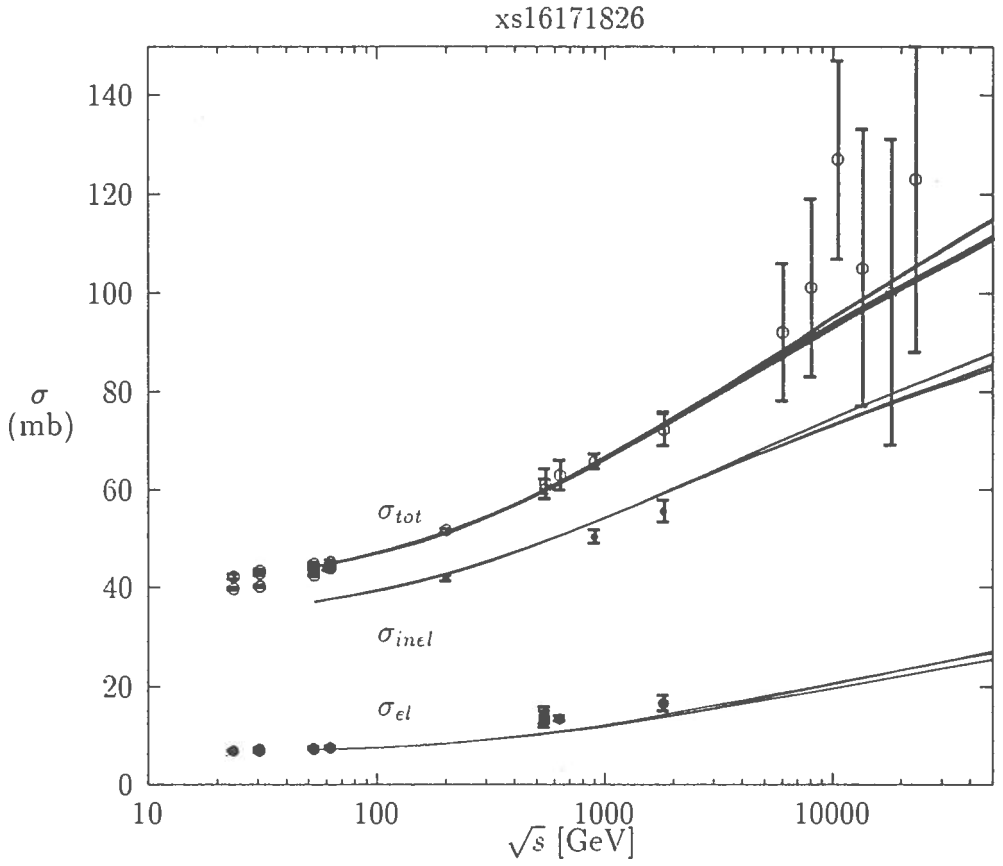

Figure 13. Cross sections σ_{tot}, σ_{el}, and σ_{in}, compared with the two-component DPM DTUJET93. (CTEQ[1M], CTEQ[1MS] and CTEQ[1ML])

with $p_\perp$ bigger than $p_{\perp thr}$ as function of $p_{\perp thr}$. The plots are given before and after the parton evolution. The curves refer to the models with the CTEQ[1ML] and the MRS[D–] parton distributions.

We observe: at 0.2 and 1.8 TeV the distributins according to these two structure functions are nearly identical, at these energies we use the structure functions in x–regions, where experimental data are available and all structure functions agree largely. While in the distributions before the final state parton evolution the structure at $p_\perp = p_{\perp thr}$ is always visible, the curves become rather smooth after the parton evolution. As to be expected, the parton evolution decreases the distributions at large $p_\perp$ values and increases the distributions at small $p_\perp$ values.

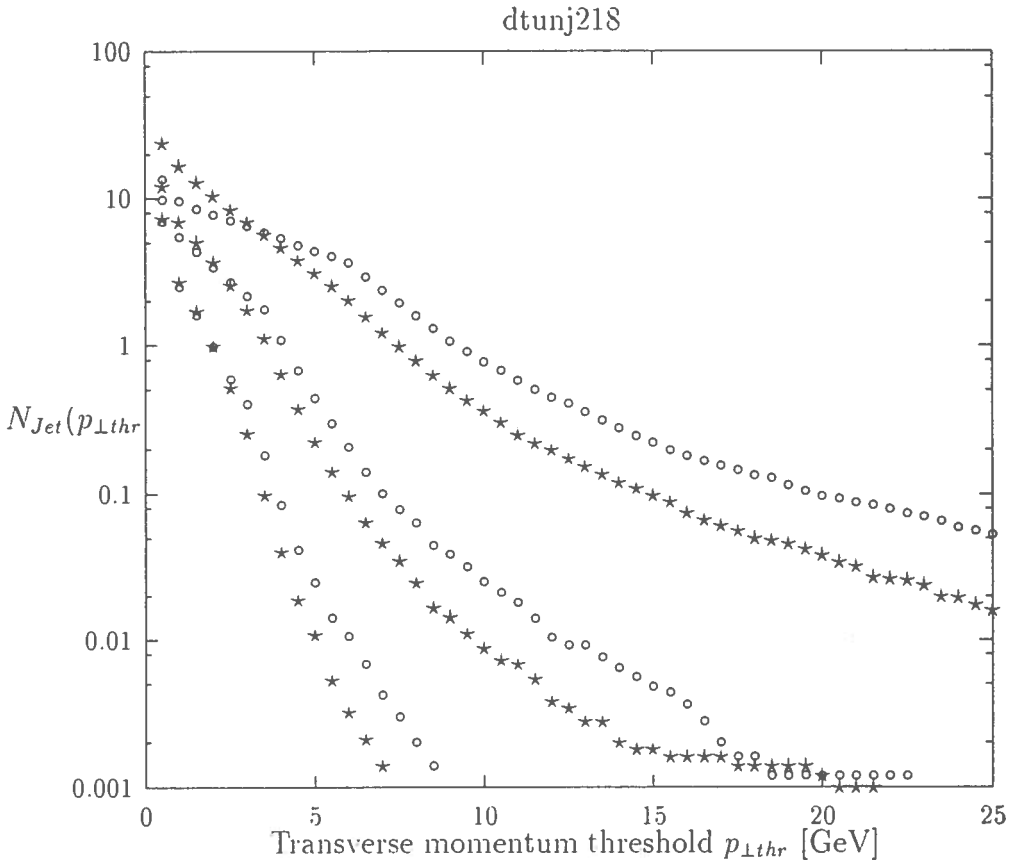

Figure 14. Number of jets with $p_\perp \geq p_{\perp thr}$. DTUJET93 with CTEQ[1ML]. Open symbols: model without parton evolution, solid symbols: model with parton evolution. The energies for the three sets of curves are from top to bottom: $\sqrt{s}$ = 40 TeV, 1.8 TeV and 0.2 TeV.

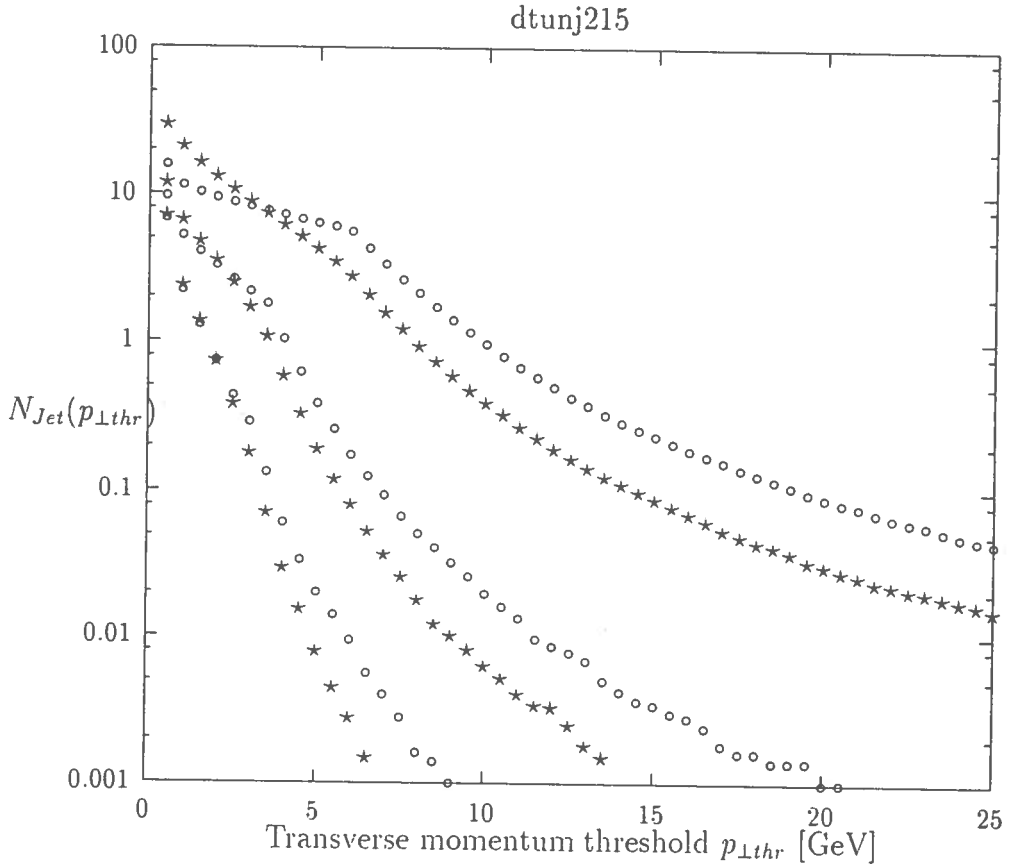

Figure 15. Number of jets with $p_\perp \geq p_{\perp thr}$, DTUJET93 with MRS[D–]. Open symbols: model without parton evolution, solid symbols: model with parton evolution. The energies for the three sets of curves are from top to bottom: $\sqrt{s}$ = 40 TeV, 1.8 TeV and 0.2 TeV.

7. Multiparticle production with DTUJET93

We get again a good phenomenology with all the known results at the CERN and TEVATRON collider.

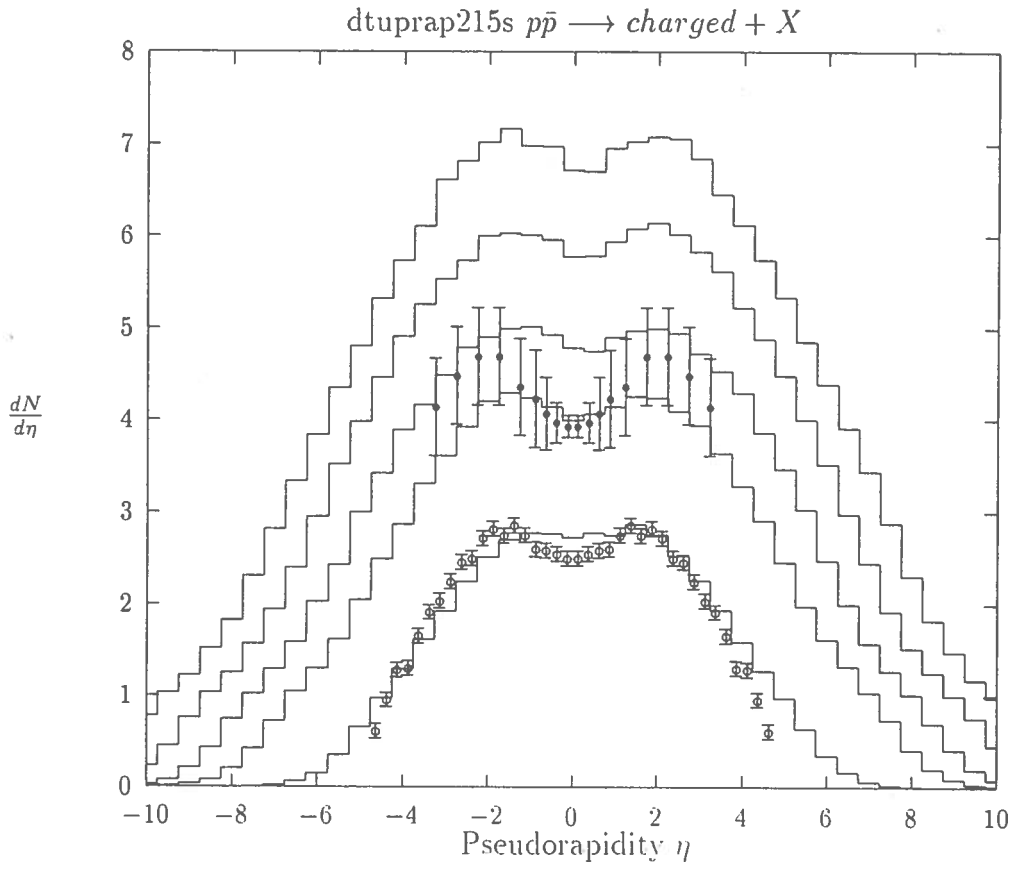

Figure 16. Pseudorapidity distributions in DTUJET93 with MRS[D−], compared to collider data[37, 38] and extrapolated to TeV energies . From top to bottom the energies are: $\sqrt{s}$ = 40 TeV, 14.6 TeV, 5 TeV, 1.8 TeV, 0.2 TeV.

In Fig.16 we compare the pseudorapidity distributions obtained in the model with the MRS[D−] parton distributions with data at collider energies[37, 38] and give the extrapolation up to LHC−energies and beyond. In Fig.17 we give the same comparison using the model with the CTEQ[1ML] parton distributions. The agreement with the data is similar in both cases, while there are slight difference in the extrapolations into the TeV energy range. It was not attempted, to determine the free parameters in the model, these are essentially some parameters in the fragmentation code , see below, to obtain an optimum agreement to the data.

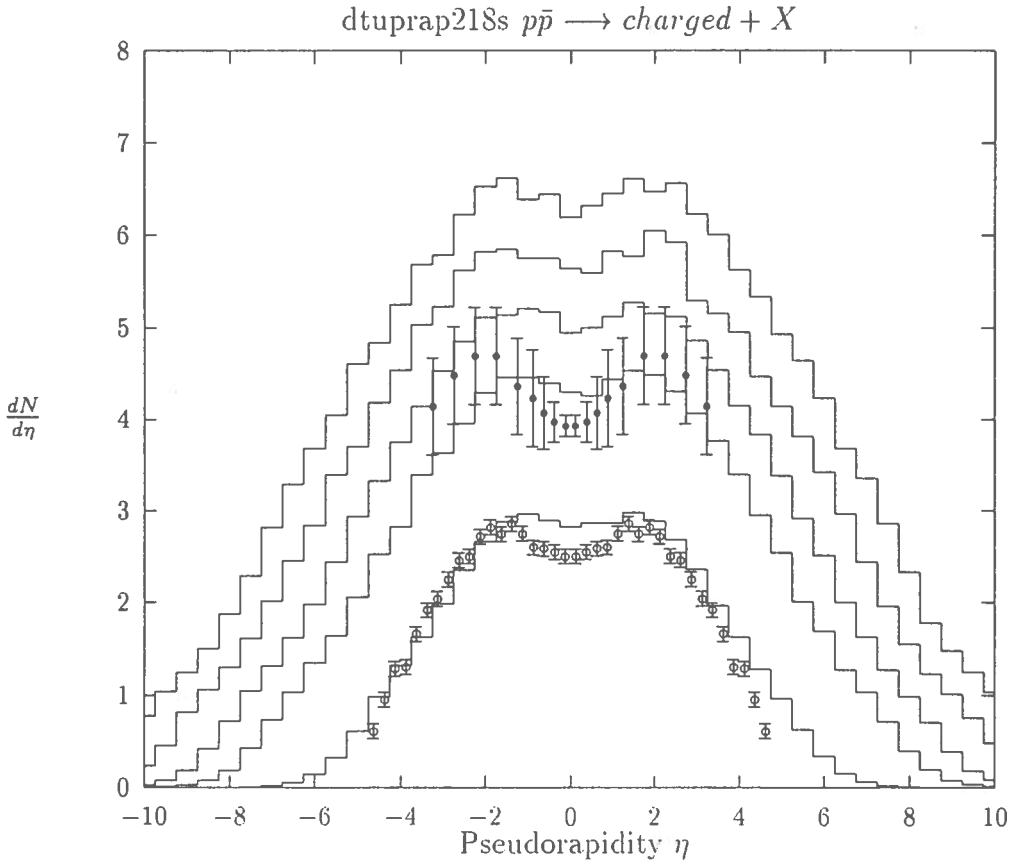

Figure 17. Pseudorapidity distributions in DTUJET93 with CTEQ[1ML], compared to collider data[37,38] and extrapolated to TeV energies . From top to bottom the energies are: $\sqrt{s}$ = 40 TeV, 14.6 TeV, 5 TeV, 1.8 TeV, 0.2 TeV.

In Fig.18 we plot the central rapidity plateau (upper three curves) and central pseudorapidity plateau obtained with DTUJET93 and the PDF's MRS[D–0], MRS[D–] and CTEQ[1ML] as function of the collision energy $\sqrt{s}$. No striking differences are seen between the three models.

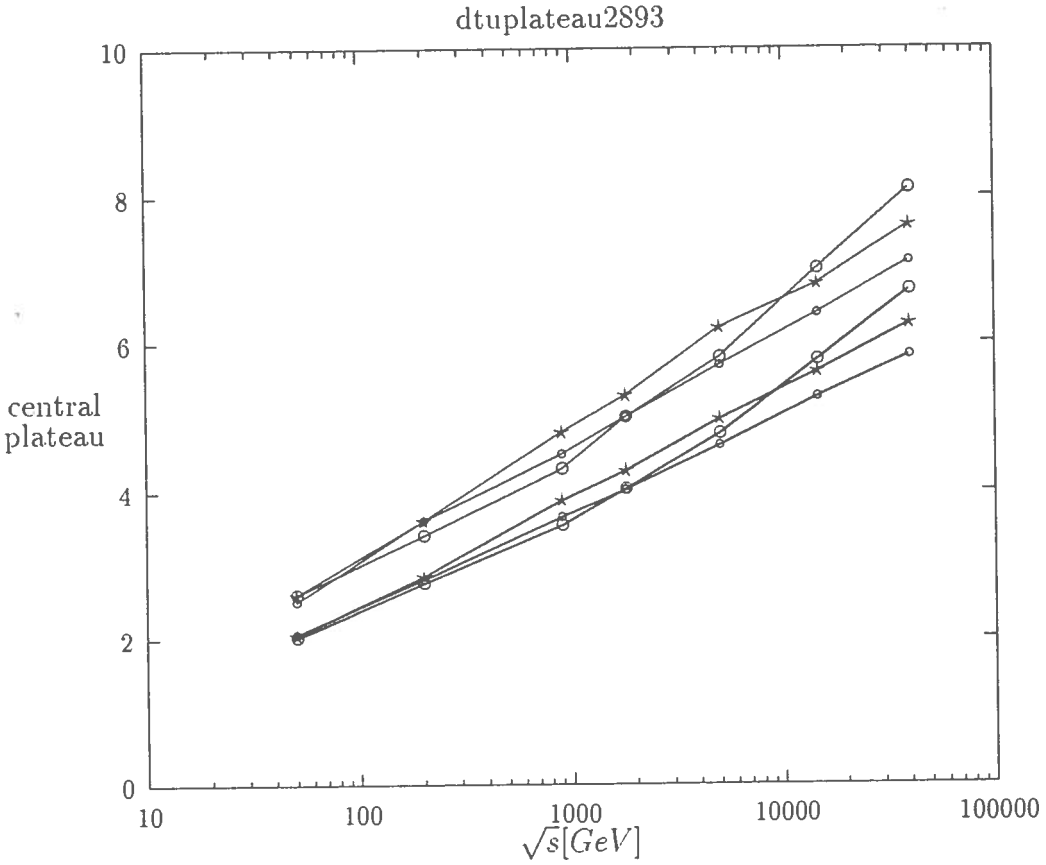

Figure 18. The rise of the central rapidity (upper three curves) and pseudorapidity (lower three curves) plateau with energy in different DTUJET93 models (MRS[D–],MRS[D–0] and CTEQ[1ML]).

In Fig.19 we plot and compare to data the average transverse momenta[39] in the central rapidity region obtained with DTUJET93 and the same three PDF's. While all three models agree well with the collider data, we find significant differences in the extrapolation into the supercollider energy region: The average $p_\perp$ rises more strongly for the more singular parton distribution functions.

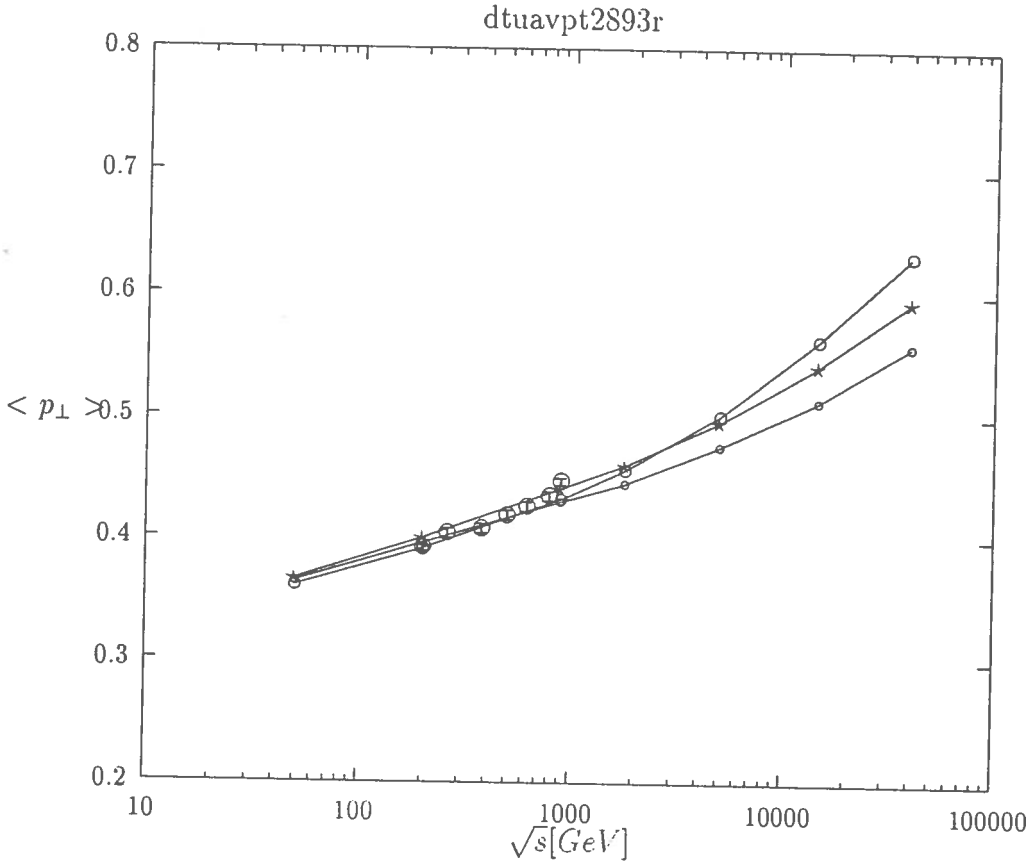

6

Figure 19. The rise of central average transverse momenta with energy in several DTUJET93 models, data from.[39] Upper curve: MRS[D–], middle curve: CTEQ[1ML], lower curve: MRS[D–0].

In Fig.20 we compare the model with UA7-data[40] for π^0– production in the fragmentation region. This is the only fragmentation region data available in the collider energy range. The agreement with the data is similar in all versions of the model.

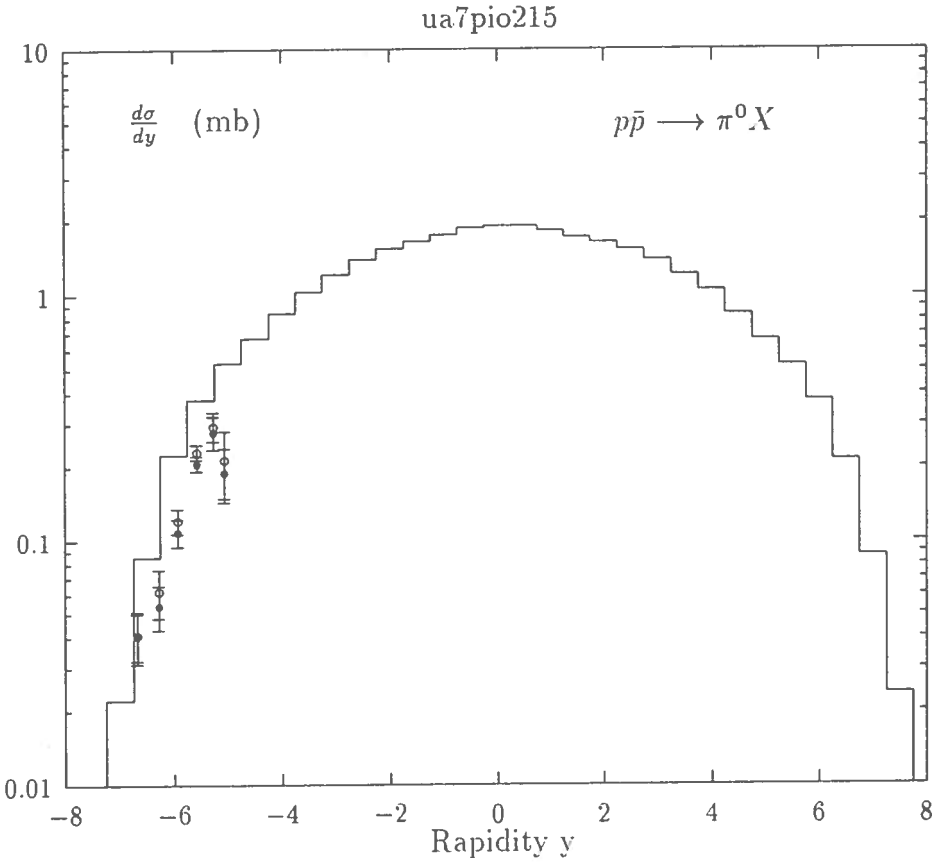

Figure 20. Rapidity distributions of π^0 in the fragmentation region in DTU-JET93 with MRS[D–], compared to collider data.[40]

In Figs.21 and 22 we compare transverse momentum distributions calculated with the models with the CTEQ[1ML] and MRS[D–] parton distributions with UA1–data.[39] The agreement is satisfactory, the model gives the correct transition between the exponential fall–off of the distributions at small $p_\perp$ to the power law fall–off at larger $p_\perp$.

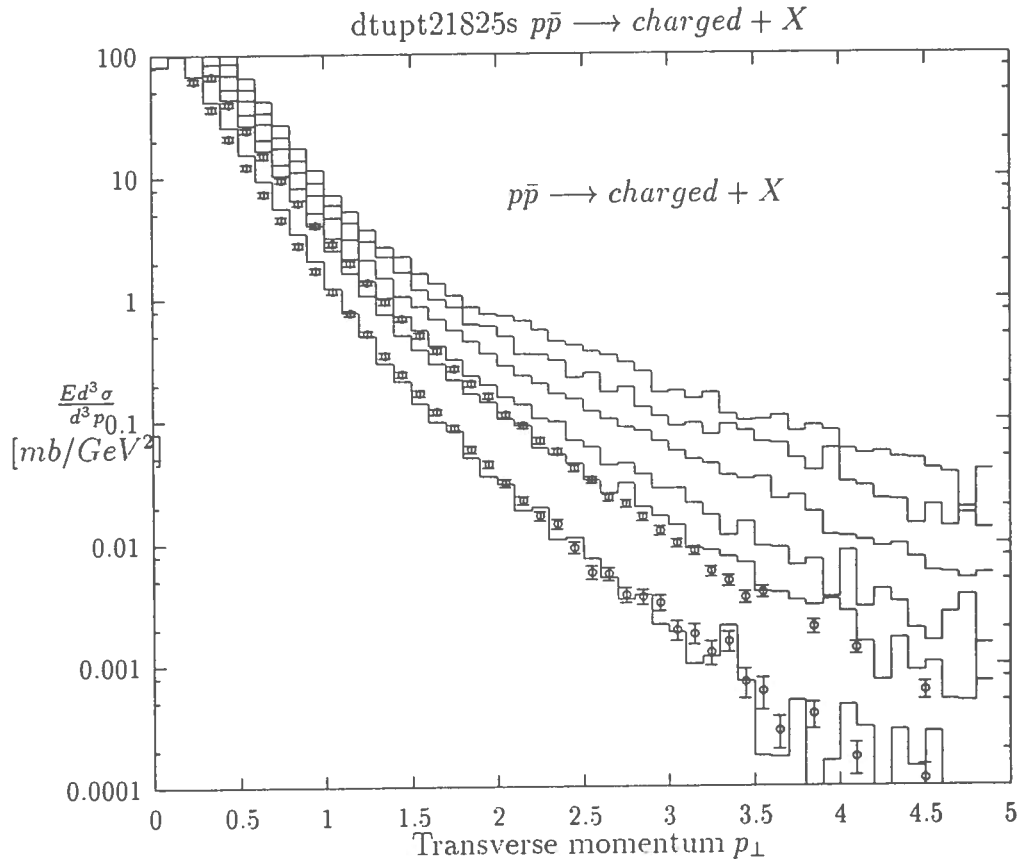

Figure 21. Comparison of transverse momentum distributions with collider data.[39] The energies are from top to bottom: $\sqrt{s}$ = 40 TeV, 14.6 TeV, 5 TeV, 1.8 TeV, 0.9 TeV and 0.2 TeV.

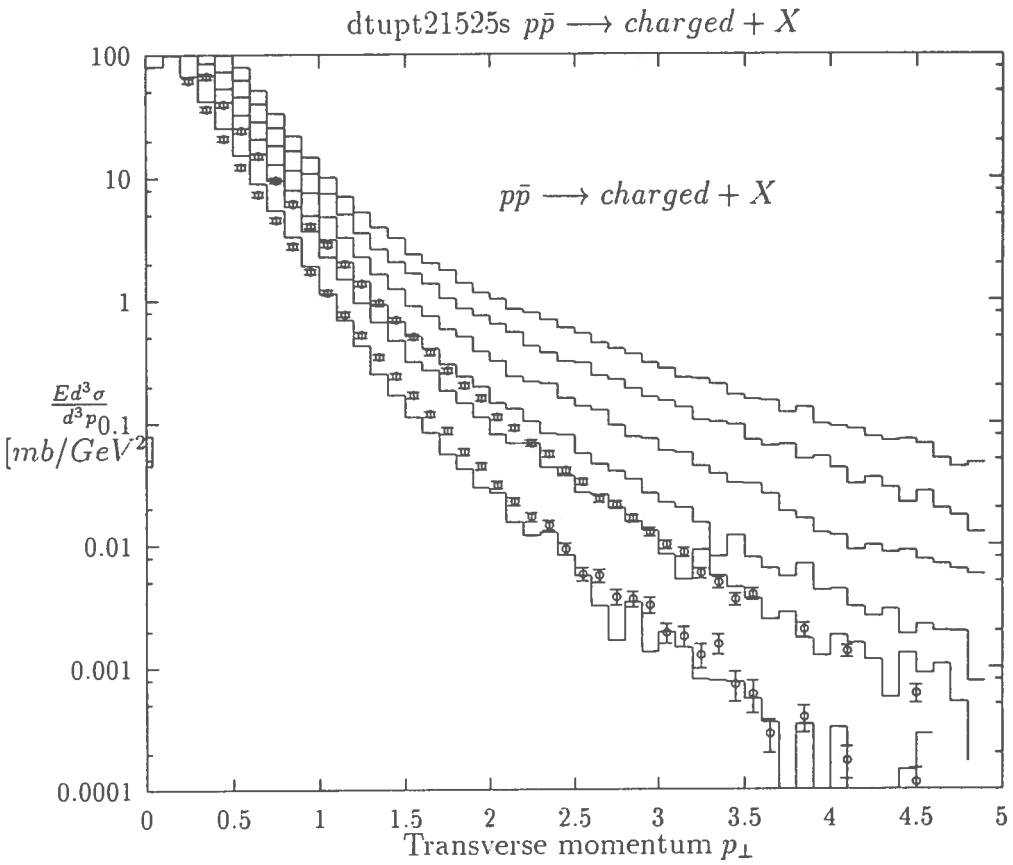

Figure 22. Comparison of transverse momentum distributions with collider data.[39] The energies are from top to bottom: $\sqrt{s}$ = 40 TeV, 14.6 TeV, 5 TeV, 1.8 TeV, 0.9 TeV and 0.2 TeV.

In Figs.23 and 24 we compare transverse energy distributions calculated with the same two parton distributions with UA1–data,[39] and we find again a reasonable agreement . These distributions are very similar to multiplicity distributions, since the average transverse momentum per produced hadron does not change much from one energy to another.

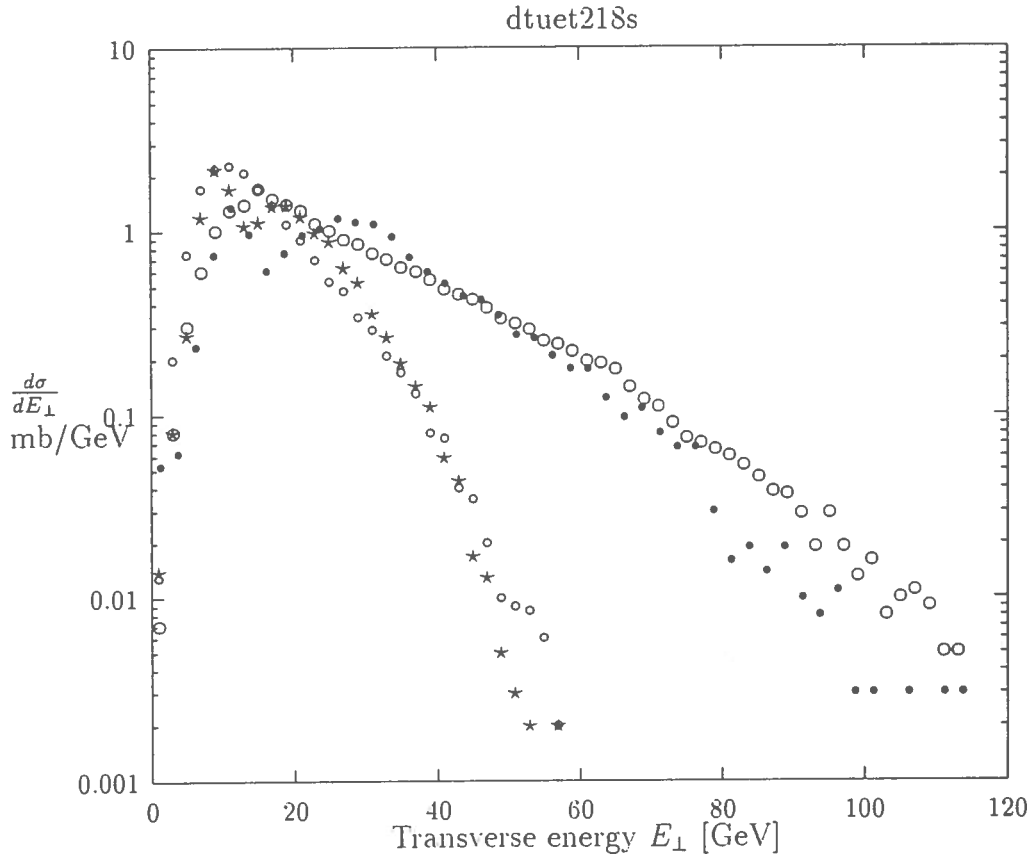

Figure 23. Comparison of transverse Energy distributions with collider data[39] . Open symbols: experimental data, solid symbols: DTUJET93. Upper curves: $\sqrt{s}$ = 900 GeV, lower curves: $\sqrt{s}$ = 200 GeV.

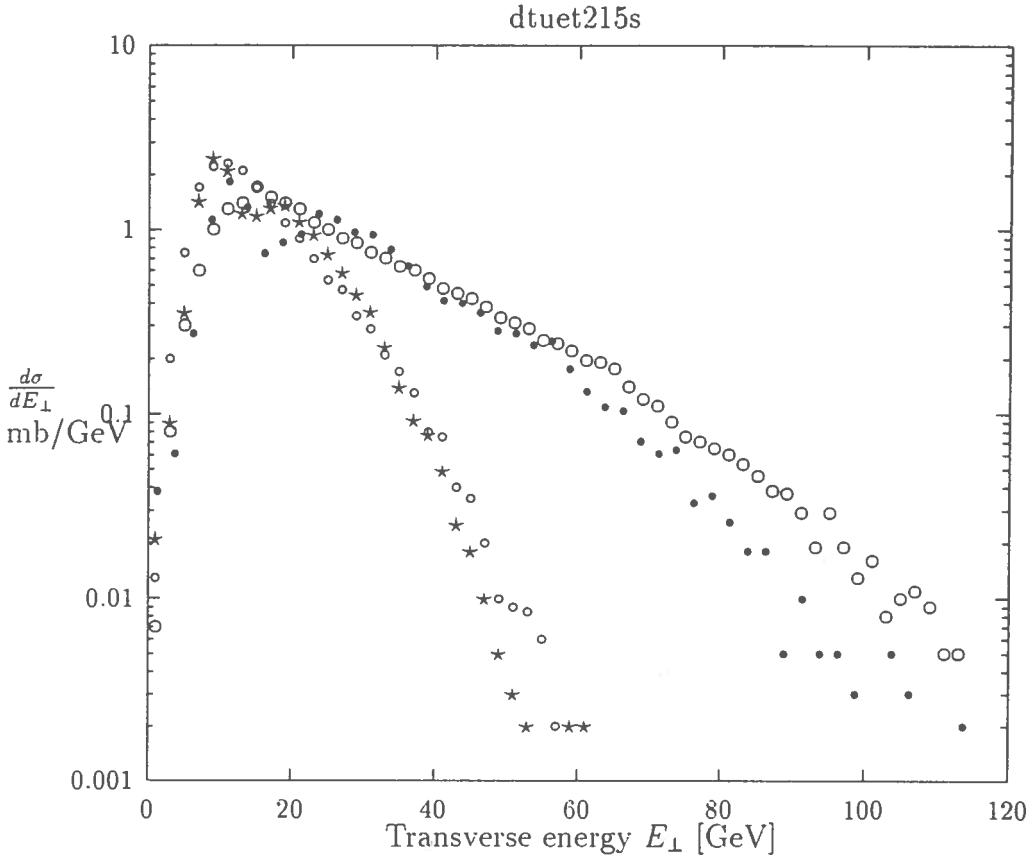

Figure 24. Comparison of transverse Energy distributions with collider data[39]. Open symbols: experimental data, solid symbols: DTUJET93. Upper curves: $\sqrt{s}$ = 900 GeV, lower curves: $\sqrt{s}$ = 200 GeV.

In Fig.25 we compare $< p_\perp >$–multiplicity correlations with data from the TEVATRON collider,[41] we get good agreement for pions and also for and antiprotons, for antiprotons the average transverse momenta rise much more strongly with multiplicity than for pions. The model is DTUJET93 with the MRS[D–] parton distribution function.

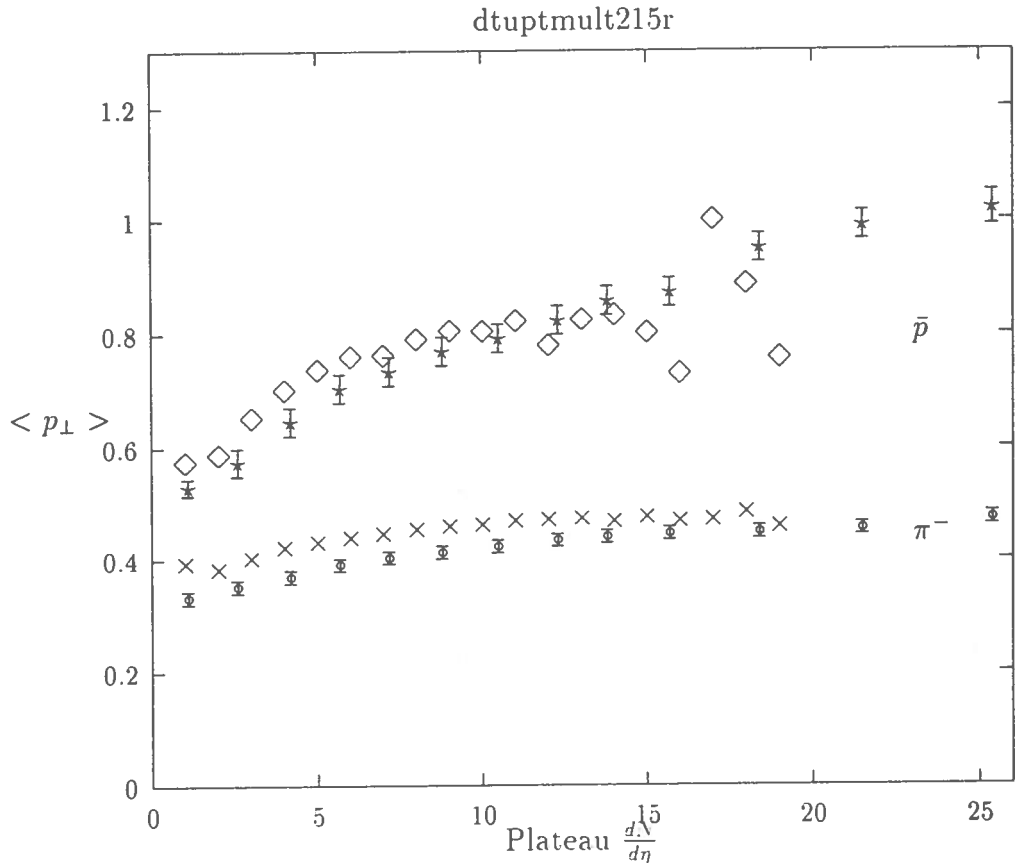

Figure 25. Comparison of average transverse momentum – multiplicity correlations with collider data.[41] The calculated values are without, the experimental data are with errorbars.

In Figs.26, 27 and 28 finally we compare the DTUJET92and DTUJET93 models with the CTEQ[1ML] parton distributions with the C_2 , C_3 and C_4 multiplicity moments as measured by the UA5-Collaboration.[42, 43] These multiplicity moments

$$C_n = \frac{< N^n >}{< N >^n}, \tag{1}$$

if not energy independent are an indication for the violation of the KNO–scaling behaviour of the multiplicity distributions.

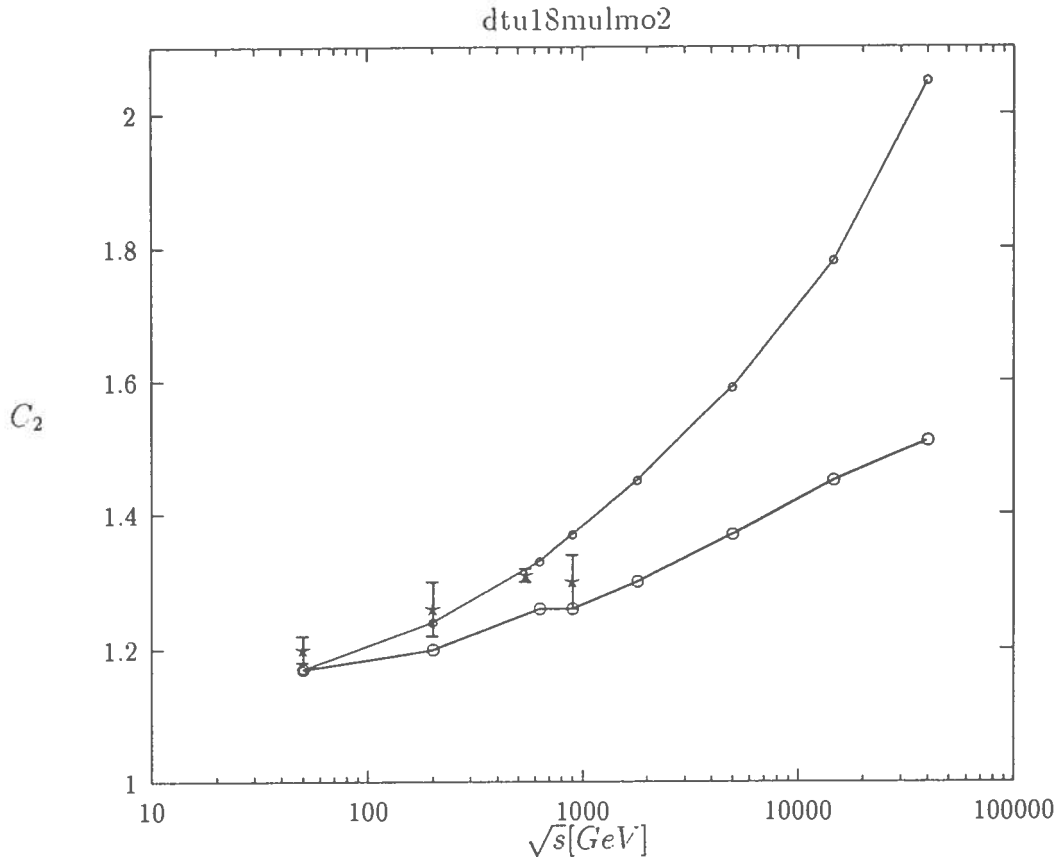

Figure 26. Comparison of multiplicity moments with collider data.[42, 43] The experimental data are with error bars, the upper curve is calculated with DTUJET92, the lower curve is calculated with DTUJET93.

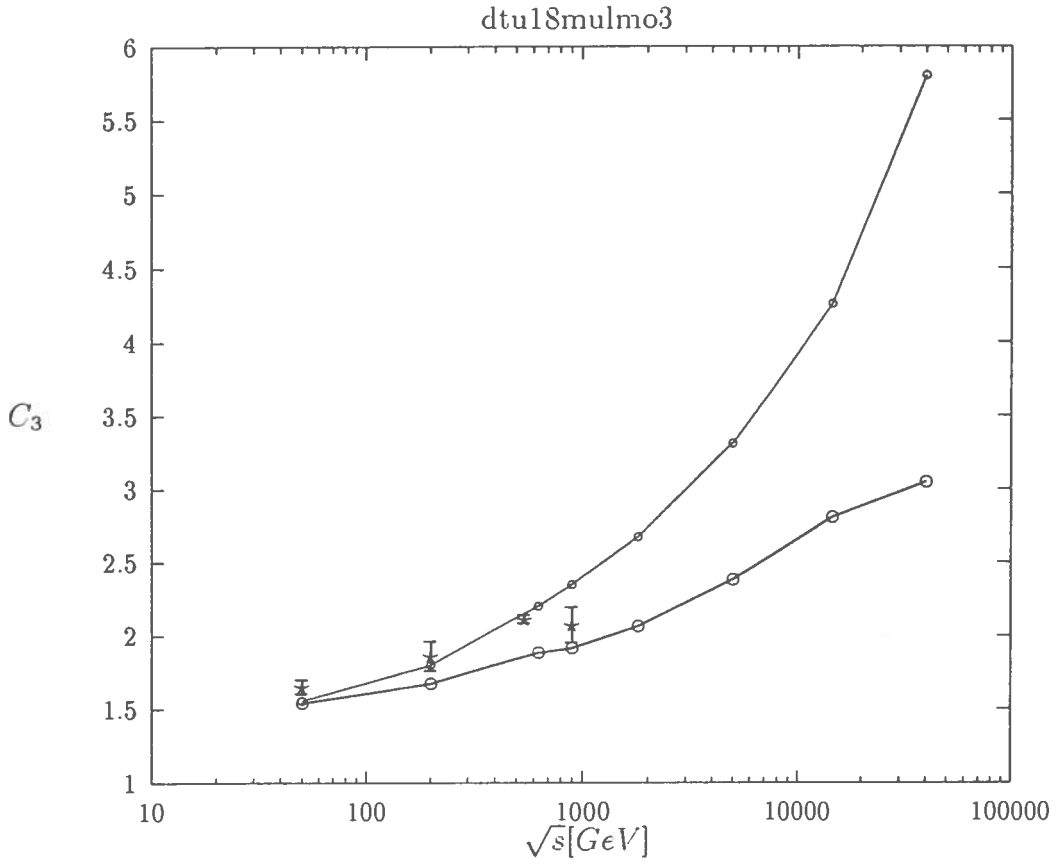

Figure 27. Comparison of multiplicity moments with collider data.[42, 43] The experimental data are with error bars. the upper curve is calculated with DTUJET92, the lower curve is calculated with DTUJET93.

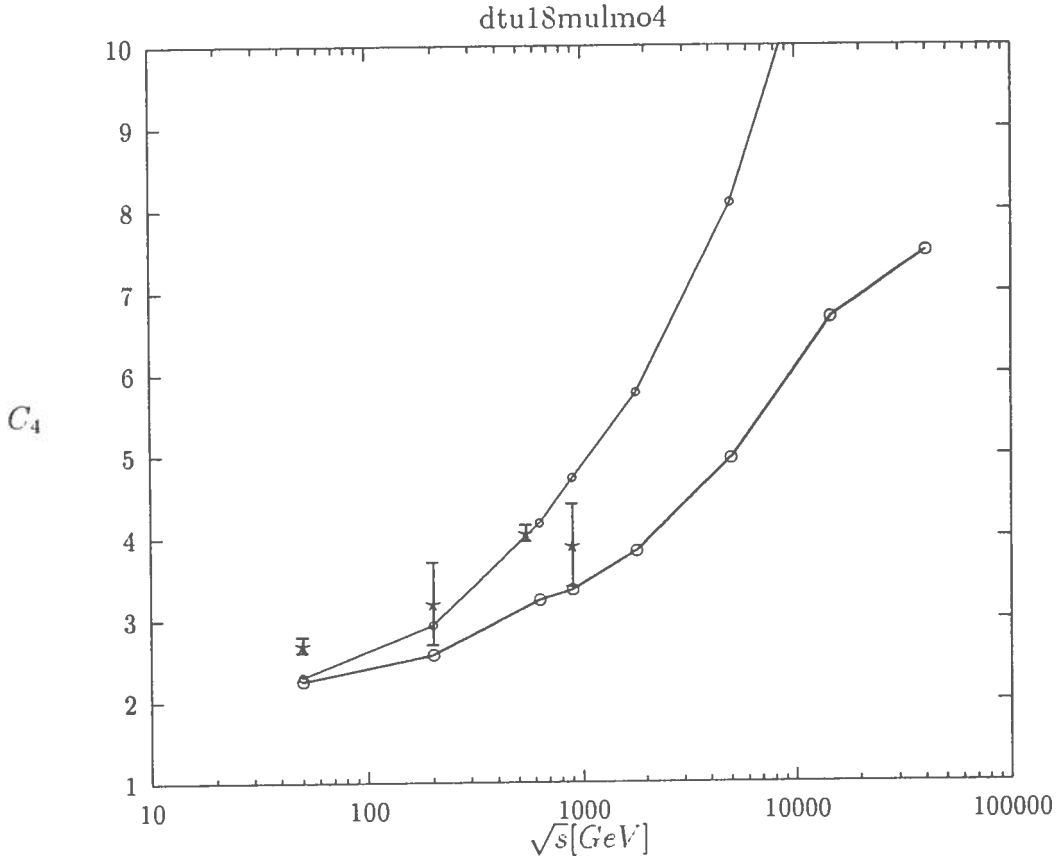

Figure 28. Comparison of multiplicity moments with collider data.[42,43] The experimental data are with error bars. the upper curve is calculated with DTUJET92, the lower curve is calculated with DTUJET93.

All distributions presented in this paper have been obtained using the Lund code JETSET-7.3[32] for the fragmentation of the strings. In the energy range considered, the parameters of JETSET are energy independent, but the best agreement to data is obtained with parameters differing slightly in DTUJET92 and DTUJET93. (For non-diffractive events in DTUJET92: PARJ(42)=3. , PARJ(21)=0.37. For nondiffractive events in DTUJET93:PARJ(42)= 1.8 , PARJ(21) = 0.45, for all other parameters we use the default parameters).

We might conclude this Section: extrapolating to LHC energies, we get charged plateaus of 5–6 particles per pseudorapidity unit for the models with all MRS-92 and CTEQ PDF's. However, the average transverse momenta in the models with the singular PDF's rise more steeply with energy than in previously published versions of DTUJET. We find using DTUJET93 at LHC energies an average $p_\perp$ typically 100 MeV/c bigger than previously.

8. Conclusions and summary

The two–component Dual Parton Model has some natural way to cut–off the singularity of the minijet cross section at low $p_\perp$. The model uses te soft Pomeron cross section as the low $p_\perp$ limit of the minijets.

With the new prescription in DTUJET93 we find the plateau rising like log s even with $1/x^{3/2}$ singular structure functions.

The average transverse momenta in this scheme rise more strongly with energy than in previous versions of DTUJET, In hadronic collisions, we get a satisfactory phenomenology at the energies of the CERN and TEVATRON colliders.

In order to get a consistent model using parton structure functions with Lipatov behaviour, we have to introduce an energy dependent transverse momentum cut–off for minijets. For nonsingular parton structure functions, the model is largely independent on this arbitrary cut–off.

9. Acknowledgements

One of the authors (J.R.) acknowledges useful discussions with B.Andersson, V.N.Gribov and A.B.Kaidalov. This work was started, when one of the authors (J.R.) was at the Dept. of Theoretical Physics at Lund. He thanks Prof. B.Andersson for the hospitality and support in Lund.

One of the authors (R.E.) acknowledges the support by the Deutsche Forschungsgemeinschaft, contract Ra 559/3–1.

REFERENCES

1. G. F. Chew and C. Rosenzweig. *Nucl. Phys.* B104(1976)290.
2. C. Hong-Mo, J. E. Paton and T. Sheung Tsun, *Nucl. Phys.* B86(1975)470.
3. A. Capella, U. Sukhatme, C. I. Tan and J. Tran Thanh Van, Orsay Preprint, LPTHE 92–38, to be published in Phys. Rep., 1992.
4. A. Capella, J. Tran Thanh Van and J. Kwiecinski, *Phys. Rev. Lett.* 58(1987)2015.
5. P. Aurenche, F. W. Bopp, A. Capella, J. Kwiecinski, M. Maire, J. Ranft and J. Tran Thanh Van, *Phys. Rev.* D45(1992)92.
6. F. W. Bopp, A. Capella, J. Ranft and J. Tran Thanh Van, *Z. Phys.* C51(1991)99.
7. F. W. Bopp, D. Pertermann and J. Ranft, *Z. Phys.* C54(1992)683.
8. R. Engel, F. W. Bopp, D. Pertermann and J. Ranft, *Phys. Rev.* D46(1992)5192.
9. S. Roesler, R. Engel and J. Ranft, *Z. Phys.* C59(1993)481.
10. B. L. Combridge, J. Kripfganz and J. Ranft, *Phys. Lett.* 70B(1977)234.
11. H.-C. Abt, T. et al., DESY preprint DESY 93–117, subm. to Nucl.Phys.B,, 1993.
12. J. Durand and H. Pi, *Phys. Rev. Lett.* 58(1987)2015.
13. X. N. Wang and M. Gyulassy, *Phys. Rev.* D44(1991)3501.
14. K. Hahn and J. Ranft, *Phys. Rev.* D41(1990)1463.
15. A. D. Martin, R. G. Roberts and W. J. Stirling, *Phys. Rev.* D47(1993)867.
16. C.-C. J.Botts et al., to be published in Phys. Lett. B, 1993.
17. E.M.Levin, to be publ. in Proc. of Aachen Conf. "QCD – 20 years later" , 1992.
18. G. Arnison et al., *Phys. Lett.* 128B(1983)336.

19. M. Bozzo et al., UA4 Collab., *Phys. Lett.* 147B(1984)392.
20. N. A. Amos et al., *Nucl. Phys.* B262(1985)689.
21. D. Bernard et al., UA4 Collab., *Phys. Lett.* 198B(1987)583.
22. G. J. Alner et al., UA5 Collab., *Z. Phys.* C32(1986)153.
23. N. A. Amos et al., E710 Collab., *Phys. Lett.* 243B(1990)158.
24. G. J. Alner et al., *Phys. Rep.* 154C(1987)247.
25. D. Bernard et al., UA4 Collab., *Phys. Lett.* 186B(1987)227.
26. J. C. M. Armitage et al., *Nucl. Phys.* B194(1982)1365.
27. R. E. Ansorge et al., UA5 Collab., *Z. Phys.* C33(1986)175.
28. D. Robinson and C. E. Wulz, UA1 Collab., Report UA1-TN / 89-10 1987.
29. N. A. Amos et al., E710 Collab., *Phys. Lett.* 301B(1993)313.
30. M. Honda et al., *Phys. Rev. Lett.* 70(1993)525.
31. R. M. Baltrusaitis et al., Fly's Eye Collab., *Phys. Rev. Lett.* 52(1984)1380.
32. T. Sjöstrand, CERN Report CERN–TH.6488/92, 1992.
33. J. Kwiecinski, A. D. Martin, R. G. Roberts and W. J. Stirling, *Phys. Rev.* D42(1990)3645.
34. Geiger, K., *Phys. Rev.* D46(1992)4965.
35. Geiger, K., *Phys. Rev.* D46(1992)4986.
36. Geiger, K., *Phys. Rev.* D47(1993)133.
37. G. J. Alner et al., UA5 Collab., *Z. Phys.* C33(1986)1.
38. F. Abe et al., CDF Collab., *Phys. Rev.* D41(1990)2330.
39. C. Albajar et al., *Nucl. Phys.* B 335(1990)261.
40. E. Pare et al., UA7 Collab., *Phys. Lett.* 242B(1990)531.
41. T. e. a. Alexopolous, *Phys. Rev.* 48(1993)984.
42. G. J. Alner et al., UA5 Collab., *Phys. Lett.* 160B(1985)193, 199.
43. R. E. Ansorge et al., *Z. Phys.* C43(1989)357.